

# HD 179821 (V1427 Aql, IRAS 19114+0002) – A Massive Post-Red Supergiant Star?

T. Şahin<sup>1,2\*</sup>, David L. Lambert<sup>2</sup>, Valentina G. Klochkova<sup>3</sup>, and Vladimir E. Panchuk<sup>3,4</sup>

<sup>1</sup> Akdeniz University, Faculty of Science, Space Sciences and Technologies Department 07058, Antalya, Turkey

<sup>2</sup> Department of Astronomy and The W. J. McDonald Observatory, The University of Texas, Austin, Texas, USA 78712

<sup>3</sup> Special Astrophysical Observatory, Nizhnij Arkhyz, Karachai-Cherkessia, 369167 Russia

<sup>4</sup> National Research University ITMO, St.-Petersburg, 197101, Russia

4 July 2016

## ABSTRACT

We have derived elemental abundances of a remarkable star, HD 179821, with unusual composition (e.g.  $[\text{Na}/\text{Fe}] = 1.0 \pm 0.2$  dex) and extra-ordinary spectral characteristics. Its metallicity at  $[\text{Fe}/\text{H}] = 0.4$  dex places it among the most metal-rich stars yet analyzed. The abundance analysis of this luminous star is based on high resolution and high quality ( $S/N \approx 120\text{--}420$ ) optical echelle spectra from McDonald Observatory and Special Astronomy Observatory. The data includes five years of observations over twenty-one epochs. Standard 1D LTE analysis provides a fresh determination of the atmospheric parameters over all epochs:  $T_{\text{eff}} = 7350 \pm 200$  K,  $\log g = +0.6 \pm 0.3$ , and a microturbulent velocity  $\xi = 6.6 \pm 1.6$  km s<sup>-1</sup> and  $[\text{Fe}/\text{H}] = 0.4 \pm 0.2$ , and a carbon abundance  $[\text{C}/\text{Fe}] = -0.19 \pm 0.30$ . We find oxygen abundance  $[\text{O}/\text{Fe}] = -0.25 \pm 0.28$  and an enhancement of 0.9 dex in N. A supersonic macroturbulent velocity of  $22.0 \pm 2.0$  km s<sup>-1</sup> is determined from both strong and weak Fe I and Fe II lines. Elemental abundances are obtained for 22 elements. HD 179821 is not enriched in s-process products. Eu is overabundant relative to the anticipated  $[\text{X}/\text{Fe}] \approx 0.0$ . Some peculiarities of its optical spectrum (e.g. variability in the spectral line shapes) is noticed. This includes the line profile variations for H $\alpha$  line. Based on its estimated luminosity, effective temperature and surface gravity, HD 179821 is a massive star evolving to become a red supergiant and finally a Type II supernova.

**Key words:** Massive star, Post-AGB stars, abundances: stars.

## 1 INTRODUCTION

The spectral class of F-G luminous giants may encompass stars on two different evolutionary paths. Some stars may be massive stars evolving from the main sequence and some of these massive stars may now be in a post-red supergiant phase. Alternatively, other stars may be departing the asymptotic giant branch (AGB) evolving at roughly constant luminosity to hotter temperatures and the tip of the white dwarf cooling track. Unambiguous assignment of a F-G supergiant to the proper evolutionary path is not always immediately possible, even when a wide variety of observational techniques are applied and the electromagnetic spectrum is well sampled.

HD 179821, also known as V1427 Aql and

IRAS 19114+0002, remains a supergiant of uncertain heritage despite a lengthy literature and frequent investigations into its status. Advocates for a post-AGB origin include Začs et al. (1996) and Reddy & Hrivnak (1999) who gave weight to their measurements of overabundances of s-process nuclides. Others have stressed the star's distance as implied by its radial velocity and characteristics of its circumstellar gas and dust shell in suggesting that the star is a massive supergiant: see, for example, Jura & Werner (1999) and Jura, Velusamy, & Werner (2001) with the latter paper carrying the provocative title ‘What next for the likely presupernova HD 179821?’. Oudmaijer et al. (2009) confidently place HD 179821 among massive stars in a post-red supergiant phase.

An oft stated assertion is that a star's chemical composition provides clues to its evolutionary history. Certainly, one anticipates readily observable distinctive signatures between an evolved massive star and a mature post-AGB star (i.e.,

\* E-mail: timursahin@akdeniz.edu.tr(TS);

dll@astro.as.utexas.edu(DLL); valenta@sao.ru(VGK)

a star that left the AGB after experiencing many thermal pulses and extensive third dredge-up episodes). The massive star will have experienced mixing between envelope and interior at a minimum and, thus, readjustment of its surface C, N and possibly O abundances: a decrease in C abundance with an offsetting increase in N abundance is assured but with very few exceptions (Na, possibly) all other elements will retain their natal abundances. On the other hand, a mature post-AGB star will be markedly *s*-process enriched with a likely enrichment of C accompanying the *s*-process enrichment. The contrasting compositions of massive and post-AGB stars surely represent a testable proposition. Unfortunately, some stars appear to evolve off the AGB before the third dredge-up has altered the surface abundances of the *s*-process nuclides (see De Ruyter et al. 2006, and references therein).

The paper is organized as follows: Section 2 discusses the high-resolution optical spectra obtained at the two observatories from 2008–2013; General properties of the spectra are discussed briefly in Section 3; Section 4 describes our abundance analysis and reanalyses previous analyses; Section 5 in a collection of concluding remarks places HD 179821 in its likely evolutionary status as a massive star evolving to become a red supergiant and finally a Type II supernova.

## 2 OBSERVATIONS

Our investigation of HD 179821 is based on high-resolution optical spectra obtained between 2008 and 2013 at two observatories: the McDonald Observatory (McD) and the Special Astrophysical Observatory (SAO). The log of observations is given in Table 1.

The character of HD 179821’s spectrum is displayed by Figure 1. Some features are blended and require spectrum synthesis to yield useful abundance information. Many lines suitable for abundance analysis are apparently unblended.

### 2.1 McDonald Observatory’s Tull spectrograph

Spectra were obtained at the W.J. McDonald Observatory with the 2.7m Harlan J. Smith reflector and the Tull coude echelle spectrograph (Tull et al. 1995). A single exposure covers the wavelength range from about 3800Å to 10 500Å. Spectral coverage is incomplete from about 5800Å to longer wavelengths. A ThAr hollow cathode lamp provided the wavelength calibration. Exposures of 20 to 30 minutes provided a satisfactory S/N ratio over much of the captured spectrum.

Observations were reduced using the software package in IRAF.<sup>1</sup> The bias level in the over scan area was modeled with a polynomial and subtracted. The scattered light was modeled and removed from the spectrum. In order to correct for pixel-to-pixel sensitivity variations, flat field exposures from a halogen lamp were used. Individual orders were cosmic-ray cleaned, and wavelength calibrated. The internal

**Table 1.** Log of observations for HD 179821 obtained at the McDonald and the SAO. S/N ratios for the SAO spectra presents the S/N values at 5500 Å while in the McDONALD spectra, the S/N values in the raw spectra are reported near 5000 Å.

Obs. Period	Exposure	Wave.Range	S/N	Notes
	(sec)	Å		
21 Apr 2008	1x1800	3877 – 10 338	174	McD
13 Jun 2008	1x1200	3832 – 10 339	193	McD
11 Jul 2008	1x1800	3833 – 10 337	136	McD
10 Aug 2008	1x1200	3833 – 10 337	154	McD
17 Aug 2008	3x2400	4550 – 6000	252	SAO
17 Sep 2008	3x1800	5260 – 6766	420	SAO
13 Apr 2009	4x2400	5214 – 6688	385	SAO
09 May 2009	1x1200	3832 – 10 338	172	McD
09 May 2009	1x1200	3832 – 10 338	172	McD
07 Nov 2009	3x3000	5220 – 6690	119	SAO
21 Nov 2009	1x1500	3832 – 10 337	166	McD
22 May 2010	1x1800	3833 – 10 337	123	McD
22 May 2010	1x1800	3833 – 10 337	123	McD
03 Jun 2010	3x2400	5210 – 6690	210	SAO
30 Jul 2010	3x2700	4422 – 5930	324	SAO
24 Sep 2010	3x1800	5220 – 6690	285	SAO
17 Nov 2010	3x2400	5160 – 6689	352	SAO
16 May 2011	1x1500	3832 – 10 338	208	McD
30 May 2013	4x0900	3916 – 6980	260	SAO
27 Aug 2013	4x2400	3917 – 6980	283	SAO
08 Oct 2013	3x2400	3914 – 6077	201	SAO

accuracy of the wavelength calibration via the ThAr lamp spectra was always better than on 0.003 Å rms. Rectification and merging of the individual orders into one spectrum were performed with bespoke echelle reduction software in IDL (Şahin 2008). The line equivalent widths (EWs) were measured in the same manner as in Şahin et al. (2011), however, one additional test was performed. The EWs were compared to those measured by using STARLINK spectrum analysis program DIPSO (Howarth et al. 1998), SPECTRE<sup>2</sup> (Snedden 1973), and an in-house developed IDL package to check any systematic errors due to continuum placement in those measurements. The results for a representative sample of weak and strong lines agreed well within  $\pm 5$  mÅ. In equivalent width measurements, the local continuum was fitted with a first-degree polynomial then equivalent widths were measured using a Gaussian profile. For strong lines, a direct integration was preferred to the Gaussian approximation. The errors for each equivalent width measurement were determined by using the prescriptions given by Howarth & Phillips (1986).

### 2.2 Special Astrophysical Observatory’s Nasymth spectrograph

Spectra were obtained with the NES echelle spectrograph (Panchuk et al. 2007, 2009) mounted at the Nasmyth focus of the 6-m telescope of the Special Astrophysical Observatory of the Russian Academy of Sciences (SAO RAS). Observations were made with a 2048 × 2048 CCD and an image slicer. For the the SAO spectra in 2013, a larger

<sup>1</sup> IRAF is distributed by the National Optical Astronomy Observatories, which is operated by the Association of Universities for Research in Astronomy (AURA), Inc., under cooperative agreement with the National Science Foundation.

<sup>2</sup> <http://www.as.utexas.edu/chris/spectre.html>

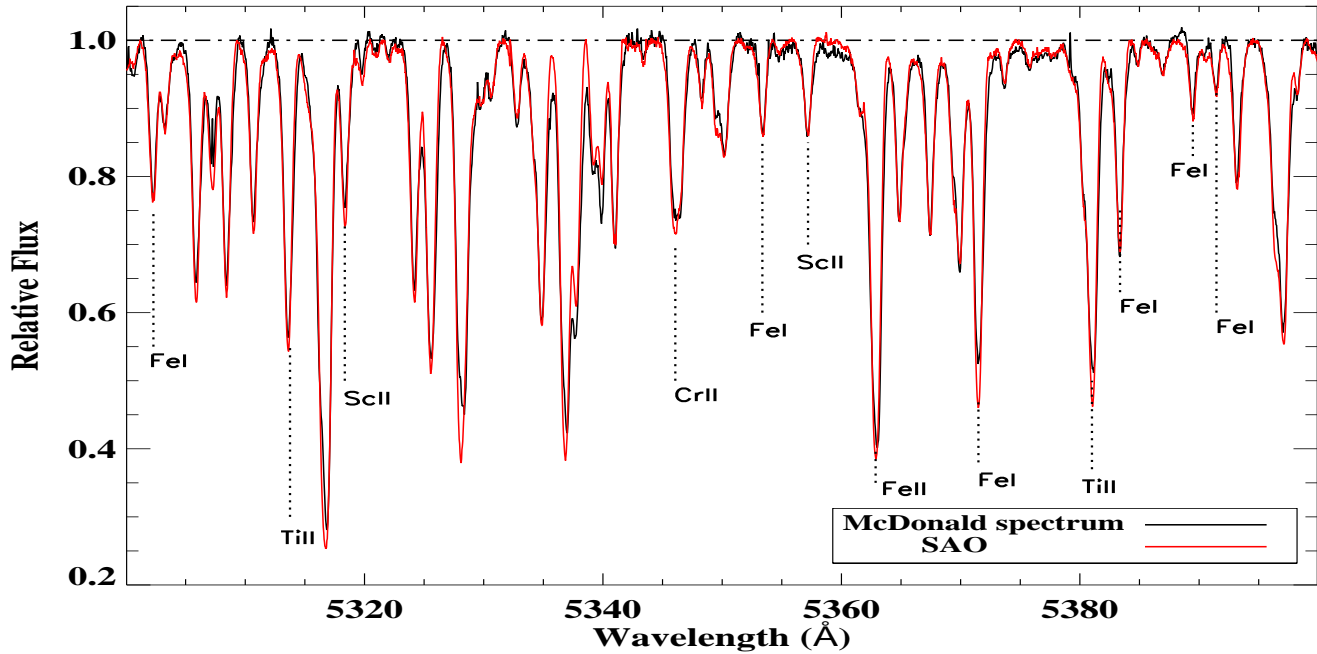


**Figure 1.** The spectrum for HD 179821 over the wavelength region 5300-5400 Å. The McDonald spectrum (13 Jun 2008) is plotted in black and the SAO spectrum (17 Nov 2010) in red.

**Table 2.** The measured heliocentric radial velocities  $V_{\text{HEL}}$  in the McDonald and the SAO spectra of HD 179821. Also, a summary of the heliocentric radial velocities of identified DIBs (SAO velocities are corrected for an offset of  $1.2 \text{ km s}^{-1}$ ) is presented (fourth column). The number of identified DIB features is included in parenthesis.

Obs. Period	HJD	$V_{\text{HEL}}$	DIB	Notes
	2450000+	$\text{km s}^{-1}$	$\text{km s}^{-1}$	
21 Apr 2008	4577.9	$91.5 \pm 0.2$	$-8.4 \pm 0.5(5)$	McD
13 Jun 2008	4630.9	$82.2 \pm 0.2$	$-8.2 \pm 0.5(5)$	McD
11 Jul 2008	4658.7	$85.7 \pm 0.2$	$-8.7 \pm 0.2(6)$	McD
10 Aug 2008	4688.6	$87.9 \pm 0.2$	$-8.4 \pm 0.7(5)$	McD
17 Aug 2008	4696.4	$88.1 \pm 0.1$	$-7.8 \pm 0.5(6)$	SAO
17 Sep 2008	4727.3	$80.0 \pm 0.1$	$-9.4 \pm 0.4(14)$	SAO
13 Apr 2009	4935.5	$88.5 \pm 0.1$	$-8.7 \pm 0.5(9)$	SAO
09 May 2009	4960.9	$87.2 \pm 0.2$	$-8.3 \pm 0.6(5)$	McD
09 May 2009	4960.9	$87.3 \pm 0.2$	$-8.7 \pm 0.4(5)$	McD
07 Nov 2009	5143.2	$84.8 \pm 0.2$	$-8.0 \pm 0.4(16)$	SAO
21 Nov 2009	5156.5	$80.5 \pm 0.3$	$-8.5 \pm 0.6(5)$	McD
22 May 2010	5338.9	$85.9 \pm 0.2$	$-8.3 \pm 0.7(4)$	McD
22 May 2010	5338.9	$86.7 \pm 0.2$	$-8.3 \pm 0.8(5)$	McD
03 Jun 2010	5351.5	$82.1 \pm 0.1$	$-9.0 \pm 0.3(15)$	SAO
30 Jul 2010	5408.4	$85.7 \pm 0.1$	$-9.3 \pm 0.0(2)$	SAO
24 Sep 2010	5464.2	$79.9 \pm 0.1$	$-9.0 \pm 0.4(9)$	SAO
17 Nov 2010	5518.2	$89.6 \pm 0.1$	$-8.9 \pm 0.8(9)$	SAO
16 May 2011	5697.9	$80.7 \pm 0.3$	$-9.1 \pm 0.7(4)$	McD
30 May 2013	6442.5	$98.1 \pm 0.1$	$-8.3 \pm 0.4(17)$	SAO
27 Aug 2013	6532.4	$86.5 \pm 0.1$	$-8.1 \pm 0.5(10)$	SAO
08 Oct 2013	6574.3	$83.5 \pm 0.1$	$-7.7 \pm 0.5(12)$	SAO

CCD ( $2048 \times 4096$ ) was employed. This provided an increase in the recorded spectral range. The spectroscopic resolution and the signal-to-noise ratio are  $R \geq 60000$  and  $S/N \geq 100$ , respectively. A modified (Yushkin & Klochkova

2005) ECHELLE context of the MIDAS package was used to extract one-dimensional vectors from the two-dimensional echelle spectra. Cosmic-ray hits were removed via median averaging of two successively taken spectra. Wavelength calibration was performed using the spectra of a hollow-cathode ThAr lamp. The NES spectra cover the wavelength range  $3916\text{\AA}$  to  $6980\text{\AA}$  without gaps and, thus, provide lines that fall in the inter-order gaps in the McDonald spectra up to almost  $7000\text{\AA}$ .

### 3 GENERAL FEATURES OF HD 179821'S SPECTRUM

A partial glimpse into the spectrum of HD 179821 is provided by Figure 1. Comparison of McDonald and SAO spectra shows that they are of matching quality. Comparison of equivalent widths of unblended lines from the McDonald spectrum for 2008 August 10 and the SAO spectrum of 2008 August 17 (a one week interval in which, we assume, the star's spectrum varied very little) shows close agreement ( $\text{EW}(\text{SAO}) = 1.01(0.01)\text{EW}(\text{McD}) - 5.95(1.94)$ ) and, thus, spectra from the two observatories may be combined to study the star's long-term behavior.

#### 3.1 $\text{H}\alpha$ profiles

Photometric variability implies spectroscopic variability. Among the striking indicators of the variability is the changing profiles of  $\text{H}\alpha$ , a variation already noted by Kipper (2008). Figure 2 shows a selection of  $\text{H}\alpha$  profiles. Weak emission in the blue or red wings is seen on occasions but a more striking change occurs in the width and radial velocity of the strong absorption line, for example, the 2010 May and July profiles are shifted to the blue by about  $20 \text{ km s}^{-1}$ .

**Table 3.** Lines used in the analysis of McDonald and SAO spectra. Abundances for individual lines are those obtained for the 2009 May 9 spectrum and a model of  $T_{\text{eff}} = 7350$  K,  $\log g = 0.64$  and  $\xi = 6.6 \text{ km s}^{-1}$ .

Species	$\lambda$	LEP	$\log(gf)$	EW	$\log \epsilon(X)$	REF <sup>a</sup>	Species	$\lambda$	LEP	$\log(gf)$	EW	$\log \epsilon(X)$	REF <sup>a</sup>
	(Å)	(eV)		(mÅ)	(dex)			(Å)	(eV)		(mÅ)	(dex)	
<i>CI</i>	4775.88	7.49	-2.304	115.0	9.14	WFD	<i>Sc II</i>	4431.33	0.61	-1.970	<i>syn</i>	4.05	NIST
<i>CI</i>	6014.84	8.64	-1.584	36.9	8.65	WFD	<i>Sc II</i>	5357.19	1.51	-2.110	75.0	3.83	NIST
<i>CI</i>	6828.19	8.53	-1.461	118.7	9.13	WFD	<i>Sc II</i>	6604.60	1.36	-1.309	227.3	3.68	NIST
<i>CI</i>	7108.92	8.64	-1.594	38.3	8.70	WFD	<i>Ti II</i>	4409.52	1.23	-2.530	<i>syn</i>	5.84	L013
<i>CI</i>	7111.45	8.64	-1.085	88.9	8.66	WFD	<i>Ti II</i>	4411.94	1.23	-2.620	<i>syn</i>	5.94	L013
<i>CI</i>	7113.17	8.64	-0.773	141.6	8.67	WFD	<i>Ti II</i>	4432.09	1.24	-3.080	<i>syn</i>	5.84	L013
<i>CI</i>	7115.17	8.64	-0.934	136.1	8.80	WFD	<i>Ti II</i>	4493.54	1.08	-2.780	<i>syn</i>	5.97	L013
<i>CI</i>	7119.70	8.64	-1.159	79.5	8.65	WFD	<i>Ti II</i>	4495.46	1.18	-3.544	<i>syn</i>	5.60	L013
<i>CI</i>	7476.15	8.77	-1.574	36.7	8.77	WFD	<i>Ti II</i>	5262.14	1.58	-2.106	<i>syn</i>	5.69	L013
<i>CI</i>	7483.41	8.77	-1.372	49.5	8.72	WFD	<i>Ti II</i>	5268.62	2.60	-1.610	<i>syn</i>	5.69	L013
<i>NI</i>	7442.29	10.33	-0.384	<i>syn</i>	9.95	WFD	<i>Ti II</i>	5418.75	1.58	-2.110	<i>syn</i>	5.84	L013
<i>NI</i>	8629.23	10.69	0.075	<i>syn</i>	9.40	WFD	<i>Cr I</i>	4646.17	1.03	-0.740	104.7	6.09	SOLS
<i>NI</i>	8594.01	10.68	-0.335	<i>syn</i>	9.80	WFD	<i>Cr I</i>	5348.33	1.00	-1.210	43.9	6.01	SOLS
<i>OI</i>	6156.77	10.74	-0.694	<i>syn</i>	9.00	WFD	<i>Cr I</i>	5409.78	1.03	-0.720	<i>syn</i>	6.02	NIST
<i>OI</i>	6158.18	10.74	-0.409	<i>syn</i>	9.08	WFD	<i>Cr II</i>	5240.92	3.76	-2.360	<i>syn</i>	6.12	NIST
<i>Na I</i>	5682.63	2.10	-0.706	<i>syn</i>	7.68	NIST	<i>Cr II</i>	5246.78	3.71	-2.460	211.9	6.20	NIST
<i>Na I</i>	5688.21	2.10	-0.452	<i>syn</i>	7.66	NIST	<i>Cr II</i>	5310.70	4.07	-2.270	180.8	6.12	NIST
<i>Na I</i>	5688.19	2.10	-1.406	<i>syn</i>	7.66	NIST	<i>Cr II</i>	5508.63	4.16	-2.120	209.3	6.19	NIST
<i>Mg I</i>	4057.48	4.35	-1.190	179.8	8.26	THEV	<i>Mn I</i>	4754.04	2.28	-0.085	105.7	5.90	NIST
<i>Mg I</i>	4167.23	4.35	-1.040	229.2	8.42	THEV	<i>Mn I</i>	4783.42	2.29	0.042	122.8	5.87	NIST
<i>Mg I</i>	4702.99	4.35	-0.550	301.0	8.34	THEV	<i>Mn I</i>	6016.64	3.07	-0.183	<i>syn</i>	5.83	NIST
<i>Mg I</i>	5528.41	4.35	-0.470	308.6	8.24	THEV	<i>Mn I</i>	6021.80	3.07	0.035	<i>syn</i>	5.90	NIST
<i>Mg II</i>	7877.06	9.99	0.390	310.0	8.36	KELP	<i>Ni I</i>	4331.64	1.68	-2.100	<i>syn</i>	7.15	NIST
<i>Mg II</i>	4481.13	8.86	0.749	<i>syn</i>	8.33	KELP	<i>Ni I</i>	4829.03	3.54	-0.330	79.6	6.95	NIST
<i>Mg II</i>	4481.15	8.86	-0.553	<i>syn</i>	8.33	KELP	<i>Ni I</i>	4831.18	3.61	-0.410	76.3	7.06	NIST
<i>Mg II</i>	4481.33	8.86	0.594	<i>syn</i>	8.33	KELP	<i>Ni I</i>	5176.56	3.90	-0.440	53.6	7.10	NIST
<i>Mg II</i>	10 092.09	11.63	0.910	<i>syn</i>	8.52	SCOT	<i>Ni I</i>	6176.82	4.09	-0.529	36.3	7.13	NIST
<i>Al I</i>	8772.87	4.02	-0.349	<i>syn</i>	6.77	KELP	<i>Ni I</i>	6767.78	1.83	-2.167	41.8	7.04	NIST
<i>Al I</i>	8773.90	4.02	-0.192	<i>syn</i>	6.77	KELP	<i>Ni I</i>	7122.21	3.54	-0.050	96.2	6.75	THEV
<i>Al I</i>	8773.91	4.02	-1.495	<i>syn</i>	6.77	KELP	<i>Ni II</i>	4362.09	4.03	-2.723	<i>syn</i>	7.15	NIST
<i>Si I</i>	5645.62	4.93	-2.141	35.6	8.61	KELP	<i>Zn I</i>	4722.16	4.03	-0.390	51.3	4.97	BIEG
<i>Si I</i>	5701.10	4.93	-2.050	36.0	8.53	KELP	<i>Zn I</i>	4810.54	4.08	-0.170	103.1	5.18	BIEG
<i>Si I</i>	5708.40	4.95	-1.470	93.3	8.48	NIST	<i>Y II</i>	5119.12	0.99	-1.360	96.3	2.78	HANN
<i>Si I</i>	5772.15	5.08	-1.750	40.9	8.40	KELP	<i>Y II</i>	5200.41	0.99	-0.570	233.1	2.72	HANN
<i>Si I</i>	5797.86	4.95	-2.051	64.0	8.84	KELP	<i>Y II</i>	5728.88	1.84	-1.120	62.0	2.95	HANN
<i>Si I</i>	6125.03	5.61	-1.540	42.1	8.62	REDH	<i>Y II</i>	6613.73	1.75	-1.110	72.3	2.92	HANN
<i>SI</i>	4694.12	6.52	-1.713	65.2	7.98	PODK	<i>Zr II</i>	4208.98	0.71	-0.510	<i>syn</i>	3.75	LJUN
<i>SI</i>	4695.45	6.52	-1.871	42.8	7.92	PODK	<i>Zr II</i>	4211.87	0.53	-1.040	<i>syn</i>	3.55	LJUN
<i>SI</i>	6743.57	7.86	-1.065	63.5	8.32	PODK	<i>Zr II</i>	4370.95	1.21	-0.770	<i>syn</i>	3.40	LJUN
<i>SI</i>	6748.78	7.87	-0.638	102.6	8.20	PODK	<i>Zr II</i>	4379.78	1.53	-0.356	<i>syn</i>	3.40	KRCZ
<i>SI</i>	6757.19	7.87	-0.351	124.1	8.04	PODK	<i>Zr II</i>	4440.45	1.21	-1.040	164.8	3.45	LJUN
<i>SI</i>	10 459.41	6.86	0.030	<i>syn</i>	8.32	SCOT	<i>Zr II</i>	4496.97	0.71	-1.540	<i>syn</i>	3.55	THEV
<i>Ca I</i>	4425.44	1.88	-0.358	<i>syn</i>	6.86	NIST	<i>Zr II</i>	4661.79	2.66	-0.620	69.1	3.58	THEV
<i>Ca I</i>	4585.87	2.52	-0.187	57.7	6.58	NIST	<i>Ba II</i>	5853.69	0.60	-1.010	<i>syn</i>	2.65	MCMW
<i>Ca I</i>	5581.98	2.52	-0.710	59.5	7.06	NIST	<i>La II</i>	4333.76	0.17	-0.060	<i>syn</i>	1.57	L001
<i>Ca I</i>	5601.29	2.53	-0.690	51.7	6.97	NIST	<i>La II</i>	4322.50	0.17	-0.930	<i>syn</i>	$\leq 1.72$	L001
<i>Ca I</i>	5857.46	2.93	0.230	127.3	6.90	NIST	<i>Nd II</i>	4061.08	0.47	0.550	<i>syn</i>	2.10	DEHG
<i>Ca I</i>	6122.23	1.89	-0.315	180.1	6.89	NIST	<i>Nd II</i>	5319.81	0.55	-0.140	<i>syn</i>	2.05	DEHG
<i>Ca I</i>	6162.18	1.90	-0.089	234.3	6.98	NIST	<i>Eu II</i>	4129.70	0.00	0.220	<i>syn</i>	1.65	L001
<i>Ca I</i>	6449.82	2.52	-0.552	58.7	6.88	NIST	<i>Eu II</i>	6645.06	1.38	1.709	<i>syn</i>	1.53	L001
<i>Sc II</i>	4420.66	0.62	-2.270	197.6	4.05	NIST	<i>Eu II</i>	7426.57	1.28	0.211	<i>syn</i>	1.76	L001

(a) References for the adopted  $gf$  values: WFD-Wiese, Fuhr, Deters (1996); NIST-Atomic Spectra Database (<http://physics.nist.gov/PhysRefData/ASD/>); KRCZ-KURUCZ Atomic Spectra Database (<http://www.pmp.uni-hannover.de/projekte/kurucz/>); THEV-Thévenin (1989); KELP-Kelleher & Podobedova (2008a); REDH-Reddy & Hrivnak (1999); PODK-Podobedova, Kelleher, Wiese (2009); SOLS-Sobeck, Lawler, Sneden (2007); SCOT-Scott et al. (2015); BIEG-Biémont & Godefroid (1980); HANN-Hannoford et al. (1982); LJUN-Ljung et al. (2006); MCMW-Mcwilliam et al. (1998); L001-Lawler, Bonvallet, Sneden (2001a); DEHG-Den Hartog et al. (2003); L013-Wood et al. (2013).

**Table 4.** Fe I and Fe II lines used in the analysis of McDonald and SAO spectra. Abundances for individual lines are those obtained for the 2009 May 9 spectrum and a model of  $T_{\text{eff}} = 7350$  K,  $\log g = 0.64$  and  $\xi = 6.6$  km s $^{-1}$ .

Species	$\lambda$	LEP	$\log(gf)$	EW	$\log \epsilon(Fe)$	Species	$\lambda$	LEP	$\log(gf)$	EW	$\log \epsilon(Fe)$
	(Å)	(eV)		(mÅ)	(dex)		(Å)	(eV)		(mÅ)	(dex)
Fe I	4009.71	2.22	-1.25	192.1	7.88	Fe I	6024.07	4.55	-0.06	96.8	7.91
Fe I	4107.49	2.83	-0.88	170.2	7.87	Fe I	6027.06	4.08	-1.09	43.5	8.16
Fe I	4213.65	2.84	-1.25	87.3	7.81	Fe I	6065.49	2.61	-1.53	70.0	7.68
Fe I	4484.23	3.60	-0.86	102.8	8.07	Fe I	6393.61	2.43	-1.58	87.3	7.70
Fe I	4602.95	1.49	-2.22	151.2	8.01	Fe I	6400.01	3.60	-0.29	122.9	7.54
Fe I	4643.47	3.65	-1.15	47.8	7.98	Fe I	6411.66	3.65	-0.72	98.6	7.88
Fe I	5090.77	4.26	-0.44	101.1	8.11	Fe I	6592.91	2.73	-1.47	71.7	7.72
Fe I	5202.34	2.18	-1.84	144.2	8.10	Fe I	6841.34	4.61	-0.60	50.3	8.15
Fe I	5353.37	4.10	-0.68	77.2	8.07	Fe II	4893.82	2.83	-4.27	238.5	8.06
Fe I	5364.88	4.45	0.23	157.0	7.86	Fe II	5427.80	6.72	-1.58	91.1	7.58
Fe I	5367.48	4.42	0.44	190.7	7.78	Fe II	5813.67	5.57	-2.75	86.4	7.89
Fe I	5373.71	4.47	-0.84	10.1	7.54	Fe II	5823.18	5.57	-2.99	67.9	7.99
Fe I	5383.38	4.31	0.65	259.7	7.80	Fe II	5991.38	3.15	-3.65	223.0	7.59
Fe I	5393.18	3.24	-0.72	133.9	7.76	Fe II	6113.33	3.22	-4.23	137.7	7.84
Fe I	5434.53	1.01	-2.12	234.4	7.82	Fe II	6116.06	3.23	-4.47	87.3	7.82
Fe I	5569.63	3.42	-0.49	149.4	7.74	Fe II	6129.73	3.20	-4.74	111.0	8.20
Fe I	5572.85	3.40	-0.28	209.4	7.78	Fe II	6179.40	5.57	-2.80	69.4	7.83
Fe I	5615.66	3.33	0.05	270.5	7.67	Fe II	6331.95	6.22	-2.07	124.7	7.94
Fe I	5816.38	4.55	-0.60	35.0	7.93	Fe II	6446.40	6.22	-2.08	89.4	7.75
Fe I	6020.17	4.61	-0.21	56.9	7.82						

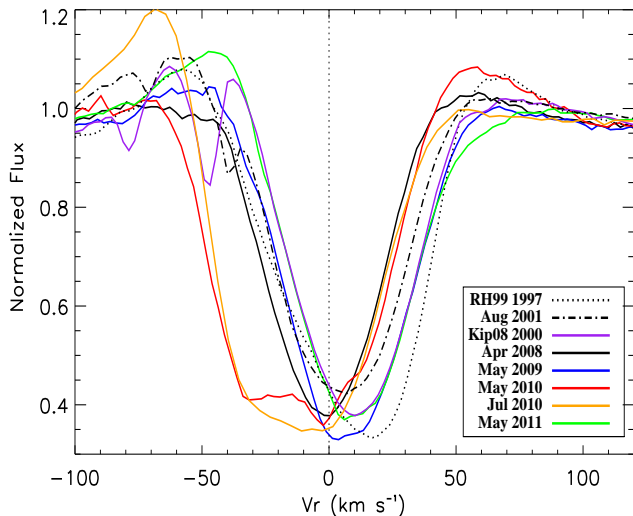


**Figure 2.** The profile of the H $\alpha$  line obtained in several observing runs. The profiles are plotted relative to photospheric velocity of the individual spectra. The ELODIE and the McDonald spectra analyzed by Kipper (2008) and Reddy & Hrivnak (1999), respectively, are also presented. The profile of H $\alpha$  in orange color is 21 July 2010 spectrum obtained by the Hobby Eberly Telescope (Luck 2016, private communication). The dot-dashed line shows the 6 August 2001 McDonald spectrum (Reddy 2016, private communication).

### 3.2 Radial Velocities

Radial velocities for the McDonald spectra were measured using cross-correlation against a spectrum of Arcturus (Hinkle et al. 2000). The spectral range used for the cross-correlation was 5300-5500Å. As a check, we also derived radial velocities from the central wavelengths of several un-

blended Fe I lines and the laboratory wavelengths (Nave et al. 1994). For a given spectrum, the two measurement techniques agreed to within about 0.4 km s $^{-1}$ . These velocities are based on the wavelength scale derived from exposures of a ThAr hollow cathode lamp observed during the same night but rarely either immediately before or after the HD 179821 exposure. To correct for a possible offset between stellar and ThAr lamp exposures, velocities were derived from telluric (H $_2$ O and O $_2$ ) lines providing a correction of 0.1-0.4 km s $^{-1}$ .

Procedures for obtaining radial velocities from the SAO spectra are described by Klochkova et al. (2008). The list of selected lines is taken from the line list for the post-AGB F supergiant HD 56126 (Klochkova et al. 2007) and again the stability of the spectrograph was checked using telluric ([O I], H $_2$ O and O $_2$ ) lines. An accuracy of 0.1-0.2 km s $^{-1}$  is achieved.

The heliocentric velocities are listed in Table 2. A variable radial velocity is evident with a peak-to-peak amplitude of about 15 km s $^{-1}$ . The central velocity and amplitude are consistent with measurements in the literature from about 10 years earlier. The mean velocity of  $85.8 \pm 0.8$  km s $^{-1}$  ( $V_{\text{LSR}} = 102.3 \pm 0.8$  km s $^{-1}$ ) from Table 2 is in good agreement with the systemic LSR velocity (100 km s $^{-1}$ ) obtained from CO observations of the expanding circumstellar shell (Zuckerman & Dyck 1986; Likkell et al. 1987; van der Veen et al. 1993; Fong et al. 2006; Castro-Carrizo et al. 2007).

Photometrically, HD 179821 is a semi-regular variable. Arkhipova et al. (2001; see also Le Coroller et al. 2003) from photometric observations of the star between 1994-1999, found low amplitude variations ( $\Delta V \simeq 0.05 - 0.20$  magnitudes) and reported the periods for fundamental pulsation ( $P_0$ ) and for the first overtone ( $P_1$ ) as 205 $^{\text{d}}$  and 142 $^{\text{d}}$ , respectively. Revised periods from UBV photometry from 2000 to 2008 by Arkhipova et al (2009) were  $P_0 = 203 \pm 5^{\text{d}}$  and  $P_1 = 141 \pm 5^{\text{d}}$ . The ratio  $P_1/P_0$  is  $\approx 0.7$ , a value of  $P_1/P_0$  is close to 0.705 in classical cepheids (Stobie 1977). Our ra-

dial velocity data are too sparse to confirm these periods but the pulsations are surely responsible for radial velocity variations.

A characteristic of all luminous supergiants is the large width of photospheric lines. HD 179821 is no exception; the line profiles provide a macroturbulent velocity of  $22 \pm 2$  km s<sup>-1</sup> (see below). Although computation of the synthetic spectrum assumes that the macroturbulence is uniform across the atmosphere, the atmosphere may be more realistically spotted with a few large convection cells, as suggested by Schwarzschild (1975) for red supergiants. The appearance and disappearance of a cell among the few populating the visible surface can lead to a profile variation and a radial velocity change.

### 3.3 Photospheric line profile variations

Asymmetric line profiles are almost a common property of the spectra over all epochs and also reported by Kipper (2008). In the 2009 McDonald spectrum, the lines have almost symmetric profiles and it was selected for the abundance analysis.

The shapes of the line profiles vary with their strengths. For several relatively high excitation lines, the broadening of the line is seen to occur mainly at the long wavelength side of the line profiles and the short wavelength side of the line profiles remains almost static. On the other hand, for the low excitation lines, the broadening is observed to occur mainly at the short wavelength side of the line profiles.

Quantitative representation of the observed line profile variations are presented in Tables A1 and A2. In these tables, the measured EWs of neutral and ionized iron lines from the spectra over all epochs are listed and indicate notable changes in the spectra for 2008, 2010, and 2013 epochs. These changes seem to correlate with the episodic variation detected in the H $\alpha$  profile, for instance, for the 2010 May and July spectra.

### 3.4 Interstellar lines

Interstellar lines may prove relevant to the interpretation of HD 179821 in two ways: their radial velocities in conjunction with a model of Galactic kinematics place constraints on the star's distance and the equivalent widths of lines with an appropriate calibration may provide an estimate of the interstellar reddening, an essential ingredient in assessing the star's luminosity. For HD 179821 with its circumstellar gas and dust, there is the possibility of contamination of interstellar lines by circumstellar components, especially in the case of the Na D lines with their complex profile.

Diffuse interstellar bands (DIBs) cross the optical spectrum, as noted previously, with Kipper (2008) providing the most complete discussion. The DIBs are assumed to be of interstellar origin. Mean radial velocities from 4 to 17 DIBs are given in Table 2. The rest wavelengths for DIBs are provided by Hobbs et al. (2008). As expected, the mean velocity does not vary from spectrum to spectrum. The mean is  $-8.5 \pm 0.5$  km s<sup>-1</sup> (over all epochs), a value consistent with that obtained by Kipper (2008). The corresponding LSR velocity is  $8.1 \pm 0.5$  km s<sup>-1</sup>. An LSR velocity of 8–10 km s<sup>-1</sup> is observed in the interstellar medium (ISM) in the direction of the star in the Galaxy (Brand & Blitz 1993). This

**Table 5.** Solar abundances obtained by employing the solar model atmosphere from Castelli & Kurucz (2004) compared to the photospheric abundances from Asplund et al. (2009). The abundances presented in bold typeface are measured by synthesis while remaining elemental abundances were calculated using the line EWs.

Species	<i>This work</i>	No.	<i>Asplund</i>	$\Delta \log \epsilon_{\odot}(X)^*$
	$\log \epsilon_{\odot}(X)$ (dex)		$\log \epsilon_{\odot}(X)$ (dex)	
<i>Cl</i>	$8.45 \pm 0.15$	7	$8.43 \pm 0.05$	0.02
<i>NI</i>	$8.08 \pm 0.08$	2	$7.83 \pm 0.05$	0.25
<i>OI</i>	$8.76 \pm 0.21$	2	$8.69 \pm 0.05$	0.07
<i>NaI</i>	$6.16 \pm 0.01$	2	$6.24 \pm 0.04$	-0.08
<i>MgI</i>	$7.60 \pm 0.00$	1	$7.60 \pm 0.04$	0.00
<i>MgII</i>	<b><math>7.54 \pm 0.01</math></b>	2	$7.60 \pm 0.04$	-0.06
<i>Al</i>	<b><math>6.42 \pm 0.00</math></b>	2	$6.45 \pm 0.03$	-0.03
<i>SiI</i>	$7.55 \pm 0.07$	6	$7.51 \pm 0.03$	0.04
<i>SI</i>	$7.12 \pm 0.04$	4	$7.12 \pm 0.03$	0.00
<i>CaI</i>	$6.20 \pm 0.23$	8	$6.34 \pm 0.04$	-0.14
<i>ScII</i>	$3.11 \pm 0.09$	4	$3.15 \pm 0.04$	-0.04
<i>TiII</i>	<b><math>5.01 \pm 0.15</math></b>	5	$4.95 \pm 0.05$	0.06
<i>CrI</i>	$5.54 \pm 0.10$	3	$5.64 \pm 0.04$	-0.10
<i>CrII</i>	$5.68 \pm 0.06$	4	$5.64 \pm 0.04$	0.04
<i>MnI</i>	$5.67 \pm 0.05$	3	$5.43 \pm 0.04$	0.24
<i>FeI</i>	$7.40 \pm 0.11$	24	$7.50 \pm 0.04$	-0.10
<i>FeII</i>	$7.50 \pm 0.08$	9	$7.50 \pm 0.04$	0.00
<i>NiI</i>	$6.22 \pm 0.19$	7	$6.22 \pm 0.04$	0.00
<i>ZnI</i>	$4.66 \pm 0.26$	2	$4.56 \pm 0.05$	0.10
<i>YII</i>	$2.35 \pm 0.19$	3	$2.21 \pm 0.05$	0.14
<i>ZrII</i>	$2.71 \pm 0.10$	2	$2.58 \pm 0.04$	0.13
<i>BaII</i>	<b><math>2.13 \pm 0.00</math></b>	1	$2.18 \pm 0.09$	-0.05
<i>LaII</i>	<b><math>1.03 \pm 0.00</math></b>	1	$1.10 \pm 0.04$	-0.07
<i>NdII</i>	<b><math>1.37 \pm 0.00</math></b>	1	$1.42 \pm 0.04$	-0.05
<i>EuII</i>	<b><math>0.43 \pm 0.02</math></b>	3	$0.52 \pm 0.04$	-0.09

(\*):  $\Delta \log \epsilon_{\odot}(X) = \log \epsilon_{\odot}(X)_{\text{This work}} - \log \epsilon_{\odot}(X)_{\text{Asplund}}$

permits us to conclude that the DIBs detected in spectra of HD 179821 are, indeed, formed in the ISM, however, the negative velocity measured for this principal ISM cloud can not be used to estimate the distance of the star.

Kipper (2008) discusses two calibrations of the reddening  $E(B - V)$  versus equivalent widths of the measured DIBs. For the  $-8.5$  km s<sup>-1</sup> leading component, we obtain  $E(B - V) \simeq 1.0$ , a value in fair agreement with the estimate of 0.7 from the broad-band colors (Arkhipova et al. 2009).

Profiles of the two NaD lines were illustrated by Začs et al. (1996), Reddy & Hrivnak (1999), and Kipper (2008) – see Fig. 3. The predicted photospheric Na D1 profile for 2009 May 9 is located between absorption components 4 and 5. Components 4 and 5 are seen to vary in intensity over all epochs. Varying intensity of these components may be an indication for a circumstellar component.

Velocities of the Na D components are constant to within the measurement errors and certainly independent of the varying photospheric velocity. Component 1 has a mean velocity of  $-10.5 \pm 0.8$  km s<sup>-1</sup>. Given the uncertainty about the rest wavelengths of the DIBs, this represents satisfactory agreement between the NaD component and the principal DIB component. Components 2 to 5 may also be of interstellar origin. The Galactic rotation model of Brand & Blitz (1993) provides a crude estimate of distance to the component 2 as  $\approx 1.5$  kpc and  $\geq 6.9$  kpc for component 5.

**Table 6.** Abundances of the observed species for HD 179821 are presented for the 9 May 2009 McDonald spectrum and the model atmospheres of  $T_{\text{eff}} = 7350$  K,  $\log g = 0.64$ ,  $\xi = 6.6$  km s<sup>-1</sup>.

Element	$\log \epsilon(X)$	$\sigma_{\text{line}}$	$\sigma_{\text{abs}}$	N	$[X/H]$	$\sigma_{[X/H]}$	$[X/Fe]$	$\sigma_{[X/Fe]}$	$\log \epsilon_{\odot}(X)$
	(dex)	(dex)	(dex)		(dex)	(dex)	(dex)	(dex)	(dex)
C I	8.79	0.19	0.18	10	0.34	0.24	-0.19	0.30	8.45 ± 0.15
N I	9.48	0.14	0.24	3	1.40	0.16	0.87	0.24	8.08 ± 0.08
O I	9.04	0.06	0.06	2	0.28	0.22	-0.25	0.28	8.76 ± 0.21
Na I	7.67	0.01	0.31	2	1.51	0.01	0.98	0.18	6.16 ± 0.01
Mg I	8.32	0.08	0.32	4	0.72	0.08	0.19	0.20	7.60 ± 0.00
Mg II	8.40	0.10	0.23	3	0.86	0.10	0.33	0.21	7.54 ± 0.01
Al I	6.78	0.01	0.20	2	0.36	0.01	-0.17	0.18	6.42 ± 0.00
Si I	8.58	0.15	0.23	6	1.03	0.17	0.50	0.25	7.55 ± 0.07
Si II	8.13	0.17	0.21	6	1.01	0.17	0.48	0.25	7.12 ± 0.04
Ca I	6.89	0.14	0.33	8	0.69	0.27	0.16	0.32	6.20 ± 0.23
Sc II	3.90	0.18	0.17	4	0.79	0.20	0.26	0.27	3.11 ± 0.09
Ti II	5.80	0.13	0.21	8	0.79	0.20	0.26	0.27	5.01 ± 0.15
Cr I	6.04	0.04	0.29	3	0.50	0.11	-0.03	0.21	5.54 ± 0.10
Cr II	6.16	0.04	0.15	4	0.48	0.07	-0.05	0.19	5.68 ± 0.06
Mn I	5.86	0.04	0.27	3	0.19	0.06	-0.34	0.19	5.67 ± 0.05
Fe I	7.93	0.14	0.26	28	0.53	0.18	0.00	0.25	7.40 ± 0.11
Fe II	7.93	0.19	0.09	11	0.43	0.21	-0.10	0.28	7.50 ± 0.08
Ni I	7.03	0.14	0.25	7	0.81	0.24	0.28	0.30	6.22 ± 0.19
Ni II	7.15	0.00	0.19	1	0.93	0.00	0.40	0.18	...
Zn I	5.08	0.15	0.26	2	0.42	0.30	-0.11	0.35	4.66 ± 0.26
Y II	2.84	0.11	0.21	4	0.49	0.22	-0.04	0.28	2.35 ± 0.19
Zr II	3.53	0.12	0.15	7	0.82	0.16	0.29	0.24	2.71 ± 0.10
Ba II	2.65	0.00	0.29	1	0.52	0.00	-0.01	0.18	2.13 ± 0.00
La II	1.65	0.11	0.36	2	0.62	0.11	0.09	0.21	1.03 ± 0.00
Nd II	2.08	0.04	0.27	2	0.71	0.04	0.18	0.18	1.37 ± 0.00
Eu II	1.65	0.12	0.20	3	1.22	0.12	0.69	0.22	0.43 ± 0.02

**Table 7.** Model atmosphere parameters from McDonald and SAO spectra.

Obs. Period	<i>This Work</i>			
	$T_{\text{eff}}$	$\log g$	$[Fe/H]$	$\xi$
	(K)	(c.g.s)	(dex)	(kms <sup>-1</sup> )
21Apr2008	7300 ± 100	0.50 ± 0.25	0.25 ± 0.15	9.1 ± 1.5
13Jun2008	7300 ± 100	0.50 ± 0.25	0.38 ± 0.15	7.2 ± 1.4
11Jul2008	7300 ± 120	0.55 ± 0.30	0.30 ± 0.17	6.8 ± 1.3
10Aug2008	7250 ± 130	0.50 ± 0.27	0.20 ± 0.19	7.7 ± 1.7
17Aug2008	7350 ± 80	0.53 ± 0.18	0.50 ± 0.12	5.4 ± 1.3
17Sep2008	7400 ± 100	0.50 ± 0.13	0.20 ± 0.14	7.6 ± 0.9
14Apr2009	7400 ± 150	0.60 ± 0.23	0.30 ± 0.17	7.8 ± 1.2
09May2009	7350 ± 200	0.64 ± 0.30	0.43 ± 0.19	6.6 ± 1.6
07Nov2009	7220 ± 80	0.50 ± 0.14	0.00 ± 0.12	6.7 ± 1.2
21Nov2009	7400 ± 120	0.60 ± 0.26	0.35 ± 0.17	8.7 ± 1.4
22May2010	7400 ± 110	0.85 ± 0.41	0.45 ± 0.18	8.9 ± 1.8
03Jun2010	7200 ± 100	0.55 ± 0.30	0.25 ± 0.15	7.4 ± 1.1
30Jul2010	7400 ± 80	0.50 ± 0.65	0.47 ± 0.45	6.0 ± 1.3
24Sep2010	7300 ± 100	0.50 ± 0.20	0.40 ± 0.14	6.4 ± 1.4
17Nov2010	7150 ± 120	0.50 ± 0.27	0.27 ± 0.14	7.7 ± 1.2
16May2011	7300 ± 130	0.50 ± 0.35	0.33 ± 0.19	7.9 ± 1.5
27Aug2013	7360 ± 130	0.72 ± 0.40	0.50 ± 0.18	8.1 ± 1.6
<b>Mean</b>	<b>7316 ± 77</b>	<b>0.56 ± 0.10</b>	<b>0.33 ± 0.13</b>	<b>7.4 ± 1.0</b>

Kipper (2008) using a calibration by Munari & Zwitter (1997) estimated the reddening provided by each Na D component. If contributions from all components are summed, the total is  $E(B - V) \simeq 0.8$ , a value in agreement with estimates from the broad band colors and the DIBs. An iden-

tification of one or more of the Na D components with the circumstellar material could change this estimate.

## 4 THE ABUNDANCE ANALYSIS

All abundance analyses were performed using standard ATLAS9 LTE model atmospheres (Castelli & Kurucz 2004)<sup>3</sup> and a recent version of the LTE line analysis MOOG code (Snedden 1973)<sup>4</sup>. All calculations assume a normal He abundance (He/H=0.085). In the following subsections, we discuss the adopted line list, the derivation of the model atmosphere parameters, and comment briefly on the obtained abundances. Then, we compare our results with previously published abundances before presenting our conclusions in Section 5 about HD 179821’s composition and its evolutionary status.

### 4.1 The line list

An essential prerequisite for the abundance analysis of HD 179821 is a set of securely identified lines with reliable atomic data. Our line lists were generated from a systematic search for unblended lines. In about 30 per cent of the accepted lines, spectrum synthesis was preferred to a direct estimate of equivalent width; known contaminating transitions in one or both wings were thus taken into account.

<sup>3</sup> <http://kurucz.harvard.edu/grids.html>

<sup>4</sup> <http://www.as.utexas.edu/chris/moog.html>

**Table 8.** Sensitivity of the derived abundances to the uncertainties of  $\Delta T_{\text{eff}} = +200$  K,  $\Delta \log g = +0.3$ , and  $\Delta \xi = \pm 1.6$  in the model atmosphere parameters for  $T_{\text{eff}} = 7350$  K,  $\log g = 0.64$ , and  $\xi = \pm 6.6$ .

Species	$\Delta \log \epsilon$			
	$\Delta T_{\text{eff}}$	$\Delta \log g$	$\Delta \xi$	$\Delta \xi$
	+200	+0.3	+1.6	-1.6
	(K)	(cgs)	(km s <sup>-1</sup> )	(km s <sup>-1</sup> )
C I	+0.15	-0.09	-0.03	+0.05
N I	-0.01	-0.03	-0.24	+0.37
O I	-0.04	0.00	-0.05	+0.04
Na I	+0.31	+0.01	-0.04	+0.45
Mg I	+0.20	-0.13	-0.21	+0.42
Mg II	+0.02	+0.05	-0.22	+0.41
Al I	+0.17	-0.10	0.00	+0.02
Si I	+0.20	-0.12	-0.01	+0.03
S I	+0.15	-0.14	-0.06	+0.02
Ca I	+0.29	-0.16	-0.04	+0.11
Sc II	+0.12	-0.04	-0.12	+0.13
Ti II	+0.15	+0.03	-0.15	+0.29
Cr I	+0.27	-0.10	0.00	+0.07
Cr II	+0.11	+0.03	-0.10	+0.26
Mn I	+0.24	-0.12	-0.02	+0.07
Fe I	+0.22	-0.13	-0.07	+0.12
Fe II	+0.07	+0.02	-0.06	+0.11
Ni I	+0.20	-0.14	-0.04	+0.02
Ni II	+0.10	+0.05	-0.15	+0.40
Zn I	+0.23	-0.12	-0.02	+0.05
Y II	+0.21	-0.01	-0.04	+0.12
Zr II	+0.14	-0.01	-0.06	+0.09
Ba II	+0.26	-0.12	-0.04	+0.06
La II	+0.35	-0.02	-0.07	+0.05
Nd II	+0.25	-0.10	-0.05	0.00
Eu II	+0.17	-0.09	-0.05	+0.03

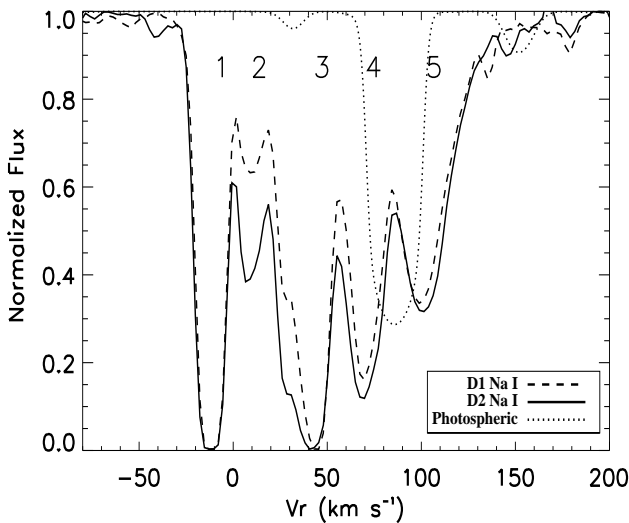


**Figure 3.** The profile of the D<sub>2</sub> (solid) and D<sub>1</sub> (dotted) lines of Na I in the McDonald 2009 May 9 spectrum of HD 179821. Telluric H<sub>2</sub>O lines have not been removed. Photospheric profile indicated with dotted line is computed for  $T_{\text{eff}} = 7350$  K and  $\log g = 0.64$ .

Our final list covers 21 elements and 141 lines over the spectra range from about 4000 Å to 10460 Å. The list of lines for elements other than Fe is provided in Table 3 with  $gf$ -values taken from the literature with references supplied in the notes to Table 3. Chosen lines of Fe I and Fe II are listed in Table 4 with  $gf$ -values taken from the critical compilation by Fuhr & Wiese (2006).

As a check on the line list and especially on the selection of  $gf$ -values, we have derived solar abundances using our list. Our lines were measured off the solar flux atlas of Kurucz et al.'s (1984) and analyzed with the solar model atmosphere from the Castelli & Kurucz (2004) grid for  $T_{\text{eff}} = 5777$  K and  $\log g = 4.44$ . Our analysis gave a microturbulence of 0.87 km s<sup>-1</sup> and the abundances in Table 5. The estimated solar abundances are compared with those from Asplund et al. (2009) in their critical review. The agreement is good but for two elements, e.g., N and Mn where our abundances are 0.25 dex greater. Perfect agreement is not expected because line lists, selection of  $gf$ -values and model atmospheres differ. In referencing stellar abundances to solar values, we use our solar abundances.

## 4.2 Model atmosphere parameters

Model atmosphere parameters – effective temperature, surface gravity, microturbulence, and metallicity – are determined from the Fe I and Fe II lines (Table 4). The selection of 28 Fe I lines range in lower excitation potential (LEP) from 1.0 to 4.6 eV with equivalent widths (EWs) of up to 270 mÅ but only four lines are stronger than 200 mÅ. Eleven Fe II lines have LEPs from 2.8 to 6.7 eV with EWs of up to 239 mÅ. Observed and computed line profiles of the chosen Fe I and Fe II lines are shown in Figures 4 and 5.

First, the temperature is estimated by requiring that derived abundances are independent of the lower excitation potential (LEP). The microturbulence  $\xi$  is derived by requiring that the derived abundances are independent of line strengths. For our sample of Fe I lines, these two conditions are imposed simultaneously. We have used Fe II lines for measuring  $\xi$  microturbulence since appreciable departures from LTE may occur for Fe I lines (Boyarchuk et al. 1985; Thévenin & Idiart 1999). In this calculation,  $\xi$  is assumed to be depth independent and isotropic. A check on the microturbulence is provided by the lines of other species using the dispersion in the abundances over a range in the  $\xi$  for a given model – see Fig. 6. The dispersion  $\sigma$  for Fe I, Fe II and Ca I lines are computed for two different effective temperature values:  $T_{\text{eff}} = 7350$  K (e.g. black curve for Fe and Ca) and 5800 K (e.g. red curve for Fe and Ca) but since  $\xi$  far exceeds the thermal velocities, the result is essentially independent of  $T_{\text{eff}}$ . We adopt  $6.6 \pm 1.6$  km s<sup>-1</sup>. An estimate of the gravity is provided by the familiar requirement that Fe I and Fe II lines provide the same Fe abundance to maintain the ionization equilibrium (Fig. 7). Since these atmospheric parameter are interdependent, several iterations have been performed to determine a suitable model from the model atmosphere grid.

The atmospheric parameters obtained are  $T_{\text{eff}} = 7350$  K,  $\log g = 0.6$ ,  $[\text{Fe}/\text{H}] = 0.4$ , and  $\xi = 6.6$  km s<sup>-1</sup>. The corresponding iron abundance is  $\log \epsilon(\text{Fe}) = 7.93$  or  $[\text{Fe}/\text{H}] \approx 0.4$  for the solar abundance of  $\log \epsilon(\text{Fe}) = 7.50$  (Asplund et al. 2009). The uncertainty in the derived surface temperature



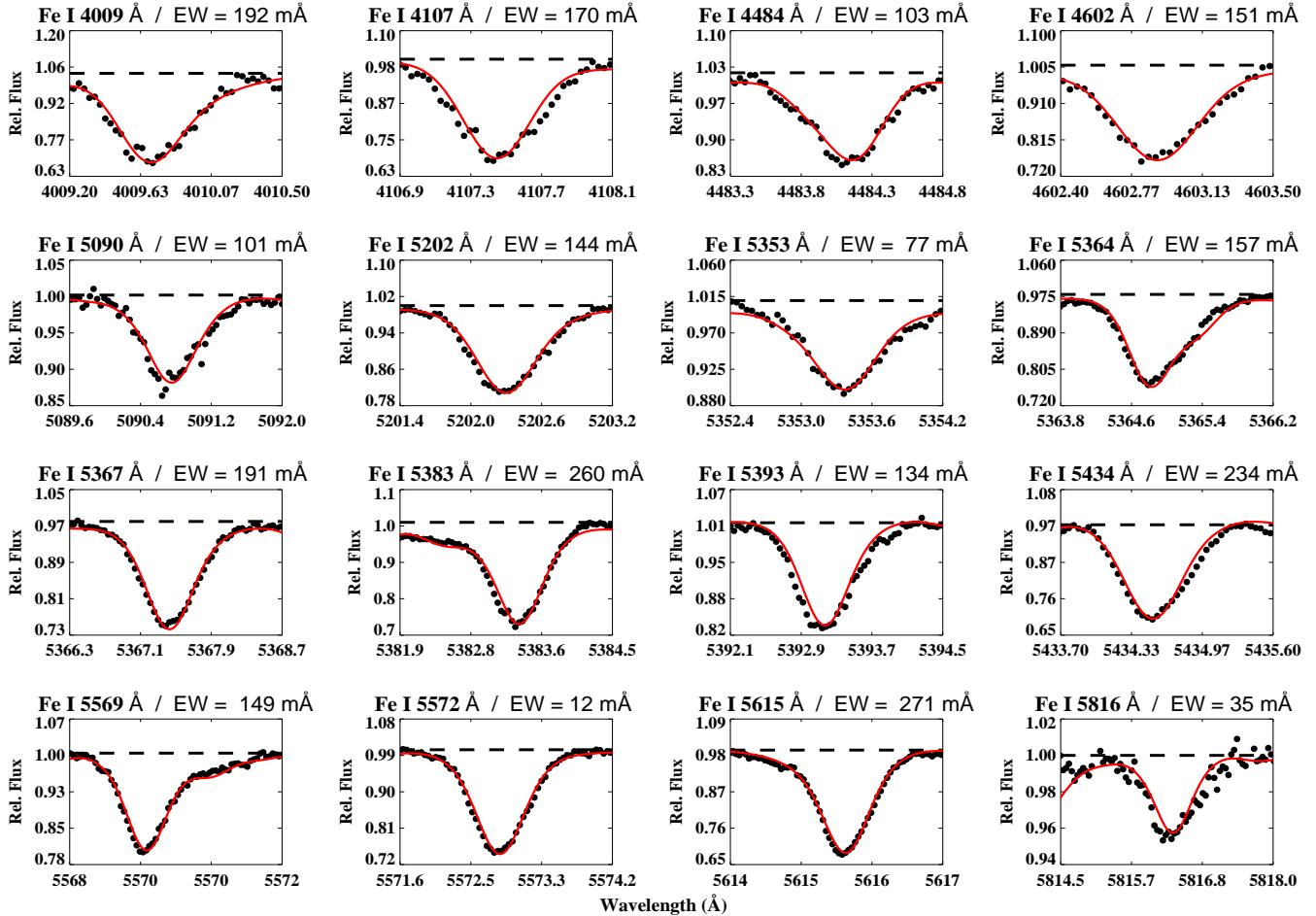


**Figure 4.** The observed (filled circles) and computed (full red line) line profiles for neutral Fe I lines used for model parameter determination from the McDonald spectrum for 2009 May 9. Their wavelengths and measured equivalent widths (EW) are indicated at the top of each panel. The computed profiles show synthetic spectra for the abundances listed in Table 4 and blending lines included as necessary.

is provided by the error in the slope of the relation between the Fe I abundance and LEPs of the lines. A perceptible change of slope occurs for a variation of  $\pm 200$  K in the adopted model (see Fig. 7 top panel). In a similar way, 1- $\sigma$  abundance difference  $[X/H]$  between neutral and ionized lines of Fe corresponds to a change of 0.3 dex in  $\log g$ . The abundances of other elements were derived (Table 6).

After having determined microturbulence, we attribute the residual broadening needed to fit the observed line profiles to macroturbulence. For determination of  $\xi_{\text{mac}}$ , we used a sample of nine relatively low excitation lines of Fe I insensitive to collisional broadening located at 5300 Å, 6000 Å, and 6100 Å. For each line, we changed  $\xi_{\text{mac}}$  until the observed half width agreed with the calculated one.<sup>5</sup> The mean  $\xi_{\text{mac}}$  resulting from this procedure after correcting for the microturbulence ( $6.6 \text{ km s}^{-1}$ ) and the instrumental width ( $5 \text{ km s}^{-1}$ ), is  $\xi_{\text{mac}} = 22.0 \pm 1.7 \text{ km s}^{-1}$ . Projected rotational velocity is assumed to be negligible.

Following analysis of the 2009 May 9 McDonald spectrum, we determined model atmosphere parameters from

all McDonald and SAO spectra – see Table 7. There is no secular trend in any of the atmospheric parameters. So, one can conclude that the line profile variations are not reflected in the atmospheric parameters. For instance, the 2010–2011 episode of H $\alpha$  broadening presented in Figure 2 is not seen in the model parameters from the McDonald and SAO spectra.

### 4.3 Balmer and Paschen lines

Additional information about the atmosphere is provided by the hydrogen Balmer and Paschen lines. At the parameters of HD 179821, the line profiles are sensitive to temperature and gravity. The variable H $\alpha$  profiles (Figure 2) are clearly highly distorted modifications of the photospheric profile. Thus, we seek to constrain the atmospheric parameters using the Balmer lines H $\beta$ , H $\gamma$  and H $\delta$  and the Paschen lines P $\delta$  at 10049 Å and P11 at 8863 Å. These profiles appear immune to the extreme variations exhibited by H $\alpha$  – see Figure 8 (top right) for a selection of spectra around the H $\beta$  line.

In the top left panel of Figure 8, we superimpose on the H $\beta$  profile for the McDonald 2009 May 9 spectrum theoretical profiles for  $[Fe/H] = +0.4$  models for  $T_{\text{eff}} = 7350 \text{ K}$  and  $\log g = 0.4$  and  $0.6$  and  $T_{\text{eff}} = 7550 \text{ K}$  and  $\log g = 0.4$ . The observed red wing is shallower than predicted suggest-

<sup>5</sup> The MOOG code computes a radial-tangential macroturbulence profile based on the work of Gray 1992, in "The Obs. & Anal. of Stell. Phot", p. 409.

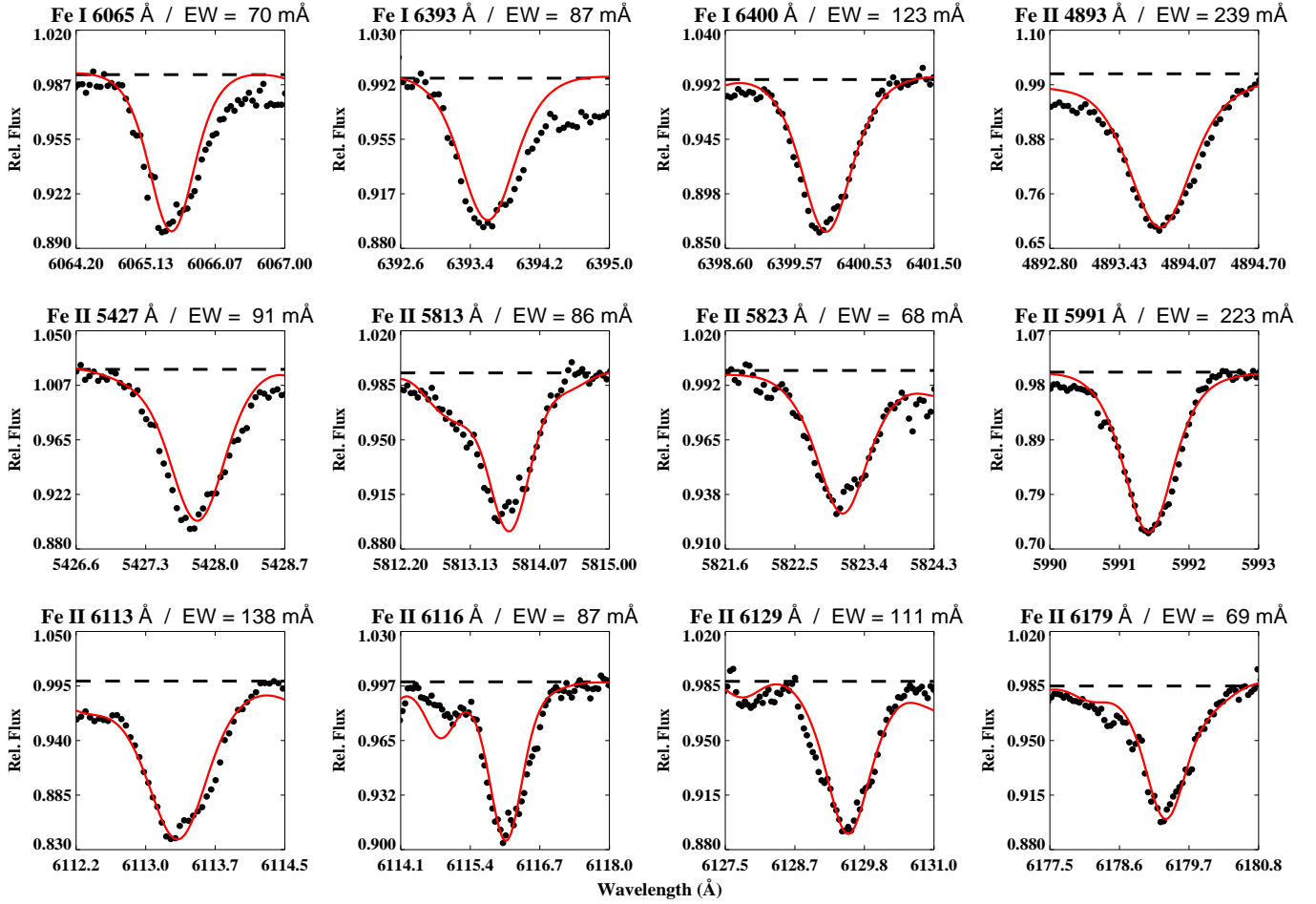


Figure 5. As in Fig.4 but Fe II lines are included (see caption to Figure 5).

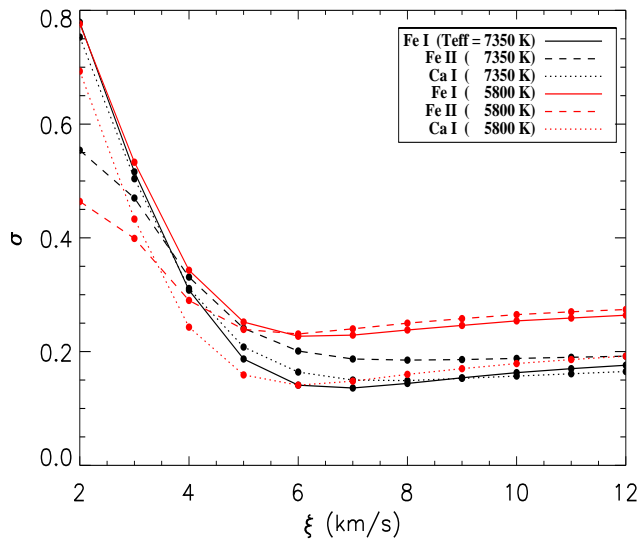
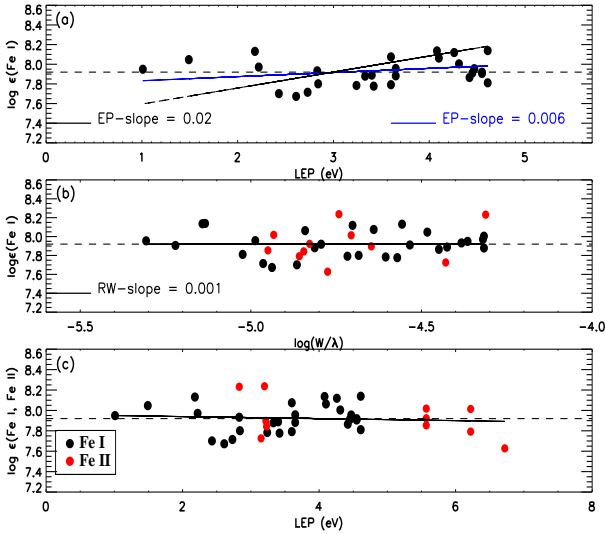


Figure 6. The standard deviation of the Fe and Ca abundances from the suite of Fe I, Fe II, and Ca I lines as a function of the microturbulence  $\xi$ .

ing that emission is affecting this wing. Predicted profiles were computed with SYNTHE and convolved with a Gaus-

sian profile in DIPSO to simulate the instrumental broadening. For all predicted profiles blending lines were computed with abundances scaled to the metallicity  $[\text{Fe}/\text{H}] = +0.4$ . These are LTE profiles but non-LTE profiles for similar supergiant atmospheres suggest that corrections for non-LTE effects affect the core of the line and are likely to be very small if collisions with hydrogen atoms are included in the statistical equilibrium calculations for the H atom (Barklem 2007; Barklem 2016, private communication). The best fit to  $\text{H}\beta$ 's blue wing is found for  $T_{\text{eff}} = 7550 \pm 200$  K and  $\log g = 0.4 \pm 0.3$ . These parameters are in fair agreement with the spectroscopic values from iron lines. Examination of a family of predicted profiles shows that  $\text{H}\beta$  can be fit by profiles along a locus in the  $(T_{\text{eff}}, \log g)$  plane from (7350, 0.3) to (7750, 0.6) through (7550, 0.4).  $\text{H}\gamma$  and  $\text{H}\delta$  as well as Paschen lines are well fitted also by the (7550, 0.4) model and other models along the locus of best-fits to the  $\text{H}\beta$  line. Emission in the red wings is absent for  $\text{H}\beta$  and  $\text{H}\gamma$  but, perhaps, weakly present for the Paschen lines (Figure 8).

Previous fits to the Balmer line  $\text{H}\delta$  gave lower temperatures which were considered to be at odds with the spectroscopic determination: Reddy & Hrivnak (1999) gave (6750, 0.5) and Kipper (2008) obtained (6000, 2.0). These estimates straddle the locus found from our fit to the  $\text{H}\beta$  line.



**Figure 7.** Determination of atmospheric parameters  $T_{\text{eff}}$ ,  $\xi$ , and  $\log g$  using abundance ( $\log \epsilon(\text{Fe})$ ) as a function of both lower level excitation potential (LEP) and reduced equivalent width (R.W.,  $\log(W/\lambda)$ ). In all the panels, the solid line is the least-square fit to the data. In (a), the solid black line is for  $T_{\text{eff}} = 7350$  K and the blue line is for  $T_{\text{eff}} = 7550$  K and in (b),  $\log \epsilon(\text{Fe})$  vs.  $\log W/\lambda$  suggests  $\xi = 6.6$  km s $^{-1}$ . In (c),  $\log \epsilon(\text{Fe I}) = \log \epsilon(\text{Fe II})$  is achieved for  $\log g = 0.6$ .

#### 4.4 The Chemical Composition

In Table 6, we present a summary of the elemental abundances based on the LTE based model parameters. In Table 6,  $\log \epsilon$  is the logarithm of the abundances. The  $\sigma_{\text{line}}$  is the  $1\sigma$  line-to-line scatter in the abundances. The  $[X/H]$  is the logarithmic abundance ratio with hydrogen relative to the corresponding solar value, and  $[X/Fe]$  is the logarithmic abundance with respect to the Fe I abundance. Estimated formal errors for the abundances arising from uncertainties of the atmospheric parameters  $T_{\text{eff}}$ ,  $\log g$ , and  $\xi$  are summarized in Table 8 for changes with respect to the model of +200 K, +0.3 cgs units, and  $\pm 1.6$  km s $^{-1}$ . From the uncertainties listed in Table 8, we find the total absolute uncertainty ( $\sigma_{\text{abs}}$ ) to be range from 0.06 for O I to 0.36 for La II by taking the square root of the sum of the square of individual errors (for each species) associated with uncertainties in temperature, gravity, and microturbulent velocity (see also column 4 in Table 6). The  $\sigma_{[X/H]}$  presents the error in  $[X/H]$  and is the square root of the sum of the quadrature of the errors in stellar and solar logarithmic abundances. The  $\sigma_{[X/Fe]}$  is the error in  $[X/Fe]$  and the square root of the sum of the quadratures of the errors in  $[X/H]$  and  $[Fe/H]$ .

Inspection of Table 6 reveals several interesting aspects of HD 179821’s composition. The mean metallicity is  $[\text{Fe}/\text{H}] = +0.33$  from all spectra - see Table 7. Luck (2014) assembled and analyzed a sample of 451 F, G, and K stars of luminosity classes I and IIa of which the vast majority are evolved intermediate mass stars and not post-AGB stars. A handful had  $[\text{Fe}/\text{H}]$  of 0.4 or greater but in conformity with expectation these stars were at Galactocentric distances inside the Solar circle. At HD 179821’s Galactic longitude of  $36^\circ$ , the line of sight at closest approach to the Galactic centre is at 5 kpc for a distance from the Sun of slightly less than 7

kpc. Given that there is an abundance gradient with higher metallicities toward the Galactic centre, a positive  $[\text{Fe}/\text{H}]$  is not unexpected. Luck and Lambert (2011) from Cepheid variables obtained the slope  $d[\text{Fe}/\text{H}]/dR_G = -0.061$  dex kpc $^{-1}$  which gives  $[\text{Fe}/\text{H}] \simeq 0.2$  for a star at 5 kpc. In Luck’s sample, almost all supergiants inside Galactocentric distances of 7 kpc have  $[\text{Fe}/\text{H}]$  of 0.3 or greater, and these values are in excess of those expected from the gradient and  $[\text{Fe}/\text{H}] = 0$  at the Sun’s Galactocentric distance of 8.5 kpc. Thus, at  $[\text{Fe}/\text{H}] = +0.4$ , HD 179821 may not be an unusual supergiant.

What may be thought unusual is that the metallicity  $[\text{Fe}/\text{H}] = +0.4$  is significantly higher than all previous spectroscopic determinations. Considering that such determinations have used spectra of comparable quality to our and methods of similar approach, it is necessary to reexamine published metallicity determinations which we do in the next section.

#### 4.5 The metallicity $[\text{Fe}/\text{H}]$

Determinations of HD 179821’s composition from high-resolution optical spectra have been reported by Začs et al. (1996), Reddy & Hrivnak (1999), Kipper (2008) and Luck (2014). Behind these (and our) analyses is a common framework involving the combination of plane-parallel model atmospheres in LTE and hydrostatic equilibrium with a line analysis programme also based on the assumption of LTE. Analyses differ by dates of the observations, the wavelength coverage of the spectra, the selection of lines and  $gf$ -values.

HD 179821 has presented two different faces to the quantitative spectroscopist: it is either metal-poor with  $[\text{Fe}/\text{H}] \simeq -0.1$  to  $-0.4$  with atmospheric parameters  $T_{\text{eff}} \simeq 6800$  K and  $\log g \simeq 0.5$  to 1.3 (Záčs et al. 1996; Reddy & Hrivnak 1999; Kipper 2008) or it is metal-rich with  $[\text{Fe}/\text{H}] \simeq +0.4$  with atmospheric parameters  $T_{\text{eff}} \simeq 7300$  K with  $\log g \simeq 0.6$  to 1.0 (Luck 2014; this paper)<sup>6</sup>.

Záčs et al. analysed a spectrum from 1992 August 17 obtained at the SAO. Abundances were given relative to those of the G8IIIab giant  $\epsilon$  Vir. With parameters  $T_{\text{eff}} = 5130$ K,  $\log g = 2.5$  and  $\xi = 2.0$  km s $^{-1}$  and  $[\text{Fe}/\text{H}] = 0$ , HD 179821 was found to be slightly Fe-poor with  $[\text{Fe}/\text{H}] = -0.1$ . However, chosen parameters for the star do not satisfy ionization equilibrium for either Fe or Cr: the reported mean Fe abundance was 7.31 from Fe I and 7.69 from Fe II lines. In light of this discrepancy, we reanalysed Záčs et al.’s line list, and obtained the model parameters:  $T_{\text{eff}} = 7300$  K,  $\log g = 0.60$ ,  $[\text{Fe}/\text{H}] = +0.40$ , and  $\xi = 6.50$  km s $^{-1}$ . These parameters are compatible with our results from McDonald and SAO spectra (Table 7).

The McDonald spectra of 1997 October 15-16 taken by Reddy & Hrivnak were analyzed using our line list. Parameters:  $T_{\text{eff}} = 7150$  K,  $\log g = 0.5$ , a microturbulence  $\xi = 9.7$  km s $^{-1}$  and  $[\text{Fe}/\text{H}] = +0.20$  were obtained. This temperature is 400 K hotter and the metallicity 0.3 dex greater than reported by Reddy & Hrivnak. Examination of the Fe lines chosen by Reddy & Hrivnak found that 9 of 23 Fe I

<sup>6</sup> Thévenin, Parthasarthy, Jasniewicz (2000)’s analysis of a low-resolution spectrum ( $R \sim 8000$ ) gave  $[\text{Fe}/\text{H}] = -0.5$  and  $T_{\text{eff}} = 5660$ K and  $\log g = -1.0$ .

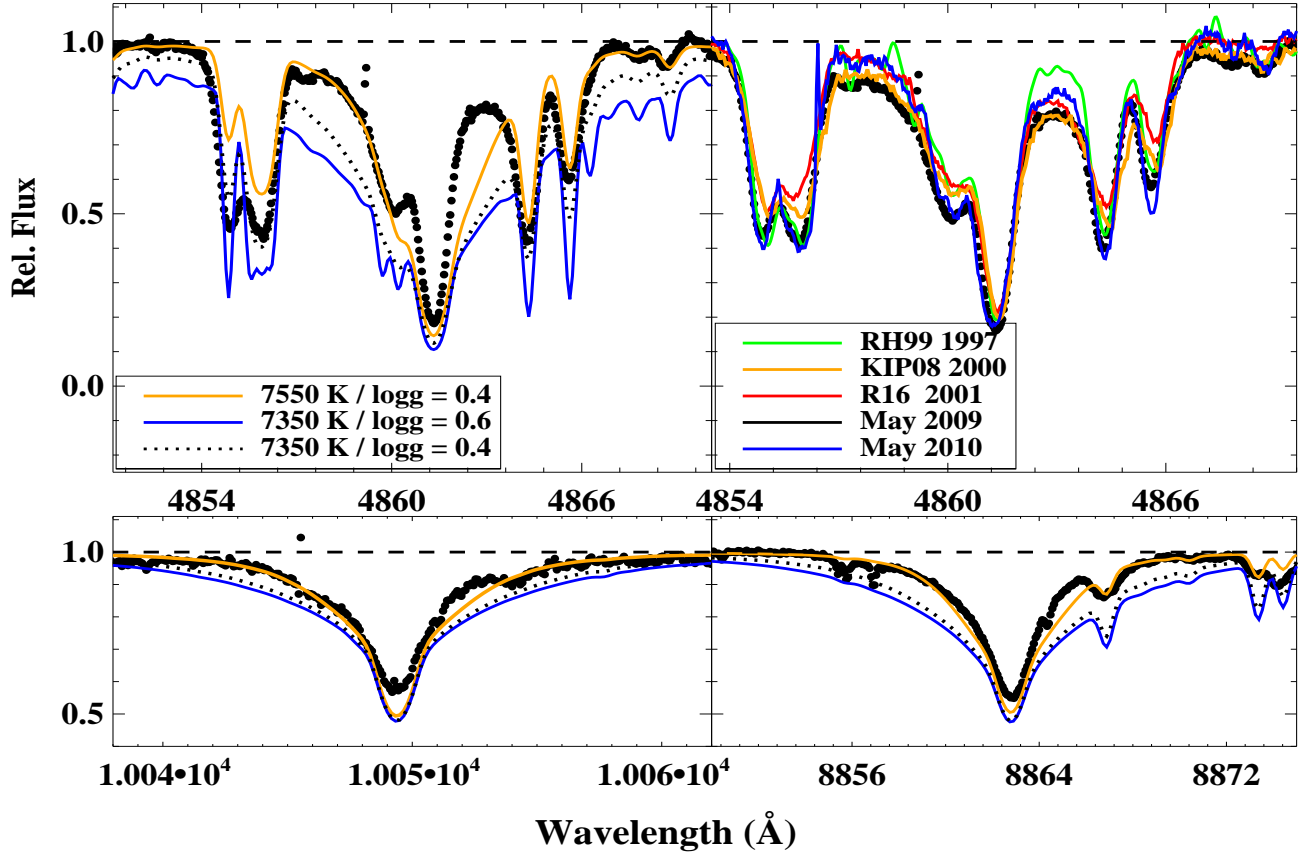


**Figure 8.** The left panel shows the observed (black dotted) and the model line profiles for  $H\beta$ . The theoretical profiles have been generated for a surface gravity  $\log g = 0.4$  and  $0.6$  dex,  $T_{\text{eff}} = 7350$  K and  $7550$  K, and  $[\text{Fe}/\text{H}] = +0.4$ . The right panel shows the observed  $H\beta$  profiles for the 1997 October McDonald spectrum (Reddy 2016, private communication), the 2000 Oct ELODIE spectrum (Kipper 2008), the 2001 August McDonald spectrum (R16; Reddy 2016, private communication), and the 2009 and 2010 May McDonald spectra. The lower panels show the observed and the model line profiles for the Paschen lines  $P\delta$  at  $10049\text{\AA}$  and  $P11$  at  $8863\text{\AA}$ .

and 3 of 9 Fe II did not meet our criteria of a measurable and unblended line. We suggest that the sub-solar Fe abundance reported by Reddy & Hrivnak likely arises from an imperfect list of Fe lines.

Kipper (2008) analyzed spectra acquired in 2000 September and October and stored in the ELODIE archive (Moultaka et al. 2004). He compiled an extensive line list which was analysed using the model selected by Reddy & Hrivnak (1999):  $T_{\text{eff}} = 6750$  K,  $\log g = 0.5$  but with a slightly higher microturbulence  $\xi = 6.6$  km s $^{-1}$ . He reported a mean Fe abundance of  $\log \epsilon(\text{Fe}) = 7.00 \pm 0.20$  from 36 Fe I lines and 11 Fe II lines but ionization equilibrium was not achieved: the Fe abundance was 6.90 from Fe I and 7.16 from Fe II lines. Relative to Asplund et al.’s solar Fe abundance, Kipper’s mean value corresponds to  $[\text{Fe}/\text{H}] = -0.5$ .

On subjecting Kipper’s line list to our analysis procedures, we found a model providing excitation and ionization equilibrium, namely  $T_{\text{eff}} = 7450$  K,  $\log g = 0.60$ ,  $\xi = 8.6$  km s $^{-1}$  with Fe abundances of  $7.88 \pm 0.17$  and  $7.87 \pm 0.22$  from the Fe I and Fe II lines, respectively, i.e.,  $[\text{Fe}/\text{H}] = +0.47$ . These parameters and Fe abundance are thoroughly compatible with our results from McDonald and SAO spectra (Table 7).

When we ran Kipper’s Fe line list through the Reddy &

Hrivnak model, we found the same lack of ionization equilibrium but higher Fe abundances than reported by Kipper. On examination of the complete line list, we found that our abundances were  $0.44 \pm 0.05$  dex greater across the array of elements; this surprising difference comes from using the same line list as Kipper in every respect and a Kurucz model with Kipper’s adopted parameters. This 0.4 dex difference is not understood. (In order to satisfy a curiosity, we extracted the 2000 ELODIE spectra used by Kipper from the archive and measured a set of clean lines and compared equivalent widths (EWs). Our measurements are in fair agreement with Kipper’s:  $\text{EW}(\text{K}) = 1.3(\pm 0.07)\text{EW}(\text{Us}) + 1.6(\pm 6.9)$ . Such EW differences have nothing to do with the 0.44 dex difference above.)

Our final comparison is with Luck (2014) who analyzed ELODIE spectra<sup>7</sup> and one taken with the High-resolution spectrograph at Hobby-Eberly Telescope (HET) at the McDonald Observatory (Tull 1998). The HET spectrum is from 2010 July 21. Luck analyzed both the ELODIE and the HET

<sup>7</sup> EWs averaged over seven ELODIE spectra, including the same spectrum as that analyzed by Kipper (2008), with the two highest S/N (153 and 180) having weight 2 and the others weight 1. (Luck 2016, private communication).

**Table 9.** Comparison of abundances of the observed species for HD 179821.

Element	This work		Luck(2014)			
	[X/Fe]	$\sigma_{\text{abs}}$	[X/Fe] <sup>1</sup>	$\sigma_1$	[X/Fe] <sup>2</sup>	$\sigma_2$
	(dex)	(dex)	(dex)	(dex)	(dex)	(dex)
C I	-0.19	0.18	-0.58	...	-0.28	0.10
N I	0.87	0.25	1.78	...	0.76	0.17
O I	-0.25	0.10	-0.38	...	0.00	0.11
Na I	0.98	0.31	1.01	0.24	0.48	0.12
Mg I	0.19	0.32	0.17	0.46	0.17	0.12
Al I	-0.17	0.20	0.16	0.00	0.15	0.16
Si I	0.50	0.23	0.26	0.13	0.20	0.03
S I	0.48	0.21	0.50	0.54	0.11	0.09
Ca I	0.16	0.33	-0.18	0.81	0.03	0.05
Sc II	0.26	0.17	0.29	0.18	0.43	0.18
Ti II	0.26	0.21	0.05	0.24	0.30	0.10
Cr I	-0.03	0.29	0.68	0.63	0.23	0.08
Cr II	-0.05	0.15	0.17	0.00	0.23	0.08
Mn I	-0.34	0.27	0.13	0.35	0.07	0.10
Fe I	0.00	0.26	-0.01	0.24	0.07	0.05
Fe II	-0.10	0.09	0.08	0.23	0.07	0.05
Ni I	0.28	0.25	0.26	0.42	0.05	0.07
Zn I	-0.11	0.26	0.09	0.55	-0.21	0.09
Y II	-0.04	0.21	0.26	0.78	0.51	0.39
Zr II	0.29	0.15	-0.04	0.34	0.24	0.18
Ba II	-0.01	0.29	-0.31	0.00	0.12	0.17
La II	0.01	0.36	-0.17	0.45	0.07	0.12
Nd II	0.18	0.27	-0.01	0.38	0.03	0.16
Eu II	0.69	0.20	0.48	0.38	....	...

(<sup>1</sup>): Mean abundances for HD 179821 from 2010 Hobby-Eberly Telescope (HET) spectrum; Luck (2014).

(<sup>2</sup>): Mean abundances from Luck (2014) for a subsample of 8 stars analysed with MARCS grids and with [Fe/H]  $\geq$  0.0 dex and  $\sigma_2$  is star-to-star scatter in [X/Fe] values.

spectra using models from two grids: the Kurucz ATLAS and the Uppsala MARCS grids. The selected ATLAS model had  $T_{\text{eff}} = 6997\text{K}$ ,  $\log g = 0.62$  and a  $\xi = 4.76 \text{ km s}^{-1}$ . The chosen MARCS model was similar with  $T_{\text{eff}} = 7107\text{K}$ ,  $\log g = 1.0$  and  $\xi = 4.74 \text{ km s}^{-1}$ . The metallicity [Fe/H] was +0.5 from the ELODIE spectrum with just a 0.03 dex difference between the values from the ATLAS and MARCS models. A slightly lower [Fe/H] value of +0.35 was obtained from the HET spectrum, again with a 0.03 dex difference between the two models. Thus, Luck’s analyses confirm our results for the atmospheric parameters and metallicity [Fe/H].

In short, reanalysis of published spectroscopic analyses show that there is general agreement that HD 179821 is metal-rich [Fe/H]  $\simeq$  +0.4. In the next section, we discuss relative abundances [X/Fe].

#### 4.6 Relative abundances [X/Fe]

In principle, HD 179821’s chemical composition may offer insights into the status of the star: a massive post-main sequence star or a lower mass post-AGB star. Obviously, such insights are compromised by uncertain and erroneous abundances. In order to minimize compromises, we pursue a multi-part discussion. We compare our abundances (Table 6) with those from Luck (2014) who, as noted above, undertook a large survey of F-G supergiants and included HD 179821.

In Table 9, we compare our [X/Fe] with the average provided by Luck from the HET spectrum and the MARCS model. Given the estimated  $\sigma$ s the comparison suggests fair agreement. A notable feature is the agreement that Na (relative to Fe) is highly overabundant, a feature noted by all previous analyses of HD 179821. In the case of Cr where Luck’s [Cr/Fe] is 0.7 dex greater than ours and his [Cr/Fe] from Cr I and Cr II lines differ by 0.6 dex, it is possible that his limited selection of Cr I lines contains blended lines.

Luck’s sample of supergiants is dominated by evolved massive stars and many have higher surface gravities than HD 179821. Yet, it is instructive to compare abundances obtained for HD 179821 with selected samples drawn from Luck’s large survey. The sample of eight stars represented in Table 9 have  $T_{\text{eff}}$  from 6600-7200 K and  $\log g$  from 1.1- 2.0. There is general agreement with our results for HD 179821, notably for C, N, and O but interesting disagreements for Na, S and Y. The high Y abundance in the sample is likely a matter of line selection given that Zr does not share the apparent overabundance,

HD 179821’s [X/Fe] may be judged against expected values for a star with [Fe/H]  $\sim$  +0.4. Abundance analyses of local dwarfs and giants show that for Na to Zn, relative abundances [X/Fe] do not differ greatly from zero, even at [Fe/H]  $\simeq$  +0.4, the metallicity of HD 179821 – see, for example, Bensby et al. 2014) for dwarfs and Luck & Heiter (2007, their Table 10) for giants. Although HD 179821’s metallicity places it at or even beyond the high metallicity limit of these samples, [X/Fe]  $\sim$  0.0 might be expected. With respect to this baseline, inspection of our and Luck’s results in Tables 6 and 9 shows the one outstanding anomaly is for Na with [Na/Fe]  $\simeq$  1.0. Possible additional anomalies include [Si/Fe], [S/Fe], [Sc/Fe], and [Ni/Fe] with [X/Fe]  $\sim$  +0.3 to +0.5. Table 6 shows that HD 179821 is not enriched in *s*-process products. Eu, an *r*-process product; appears overabundant relative to the anticipated [X/Fe]  $\sim$  0.0.

The assumption of LTE was adopted in the construction of the model atmosphere and in the analysis of the absorption lines. Given the low particle densities in the atmosphere, one should be concerned about the effects of departures from LTE on the atmospheric structure and the formation of the lines. We are unaware of supergiant atmospheres constructed in non-LTE. There are some calculations of line formation in relevant atmospheres which suggest approximate corrections to [X/H] and [X/Fe] for HD 179821. Fortunately, some results are available for the interesting light elements C, N and O. Venn (1995) in her analyses of A and F supergiants computed non-LTE corrections for selected lines of C I and N I and her stellar sample included four stars with  $T_{\text{eff}}$  between 7400-7600 K and surface gravities  $\log g$  from 1.1-1.6 with approximately solar metallicities. Considering our chosen lines and assuming that Venn’s quartet are representative of HD 179821, Venn’s calculations imply that the non-LTE abundance is about 0.3 dex for both C and N smaller than the tabulated LTE abundances. Takada & Takeda-Hidai (1998) provide non-LTE predictions for the 6157 Å lines in A-F supergiants, At the atmospheric parameters of HD 179821, their calculations show that the LTE O abundance should be reduced by 0.1 to 0.2 dex.

For abundances of species from Na to Zn, the outstanding abundance anomaly is held by Na with a 1.0 dex enrichment which may be an indicator for a high luminosity sta-

tus of the star, hence operation of Ne-Na cycle (Denissenkov & Ivanov 1987; Denissenkov 2005). Lind et al.'s (2011) extensive non-LTE calculations for Na I lines did not cover the atmospheric parameters of HD 179821 as the most extreme supergiant model was a relatively cool  $T_{\text{eff}} = 5500\text{K}$  at  $\log g = 1.0$ . By extrapolation, it would seem that the non-LTE correction to HD 179821's Na abundance is small. This suspicion is confirmed by pioneering calculations by Boyarchuk, Denisenkov, & Hubeny (1988a) and Boyarchuk et al. (1988b, c): Korotin (2016, private communication) predicts  $\Delta([Na/H]) = -0.14$  dex<sup>8</sup>. Venn's (1995) estimates for a few Mg I lines in late-F and early-F supergiants suggest only a 0.1 dex reduction of the LTE abundances but her and our selections of Mg I lines show little overlap. Extensive calculations of Mg I line formation in cool stellar atmospheres have been reported by Osorio & Barklem (2016) for many Mg I lines. Inspection of their predictions for four strong lines in Table 3 show that the non-LTE Mg abundances for a HD 179821-like model atmosphere<sup>9</sup> are about +0.2 dex greater than the LTE value. The highest correction is needed for 5528 Å Mg I line with +0.2 dex and the corrections for 4057, 4167, and 4702 Mg I lines are about +0.1 dex. These corrections are less than the uncertainty arising from the microturbulence. Non-LTE calculations for Zn I lines (Takeda et al. 2005) show a very small non-LTE abundance correction. Non-LTE effects for prominent Ba II lines in cool stars have been calculated by Korotin et al. (2015). The examined grid of stellar atmospheres extends up to 6500 K and down to  $\log g = 0$  and to stars as Fe-rich as  $[Fe/H] = +0.5$ . For the model parameters reported in Section 4.2, the non-LTE Ba abundance from the 5853 Å Ba II line for HD 179821 is +0.3 dex greater than the LTE abundance listed in Table 6 (Korotin 2016, private communication). In interpreting  $[X/Fe]$ , one obviously must consider the non-LTE corrections to the Fe abundance. In the case of Fe, a leading non-LTE effect is the over-ionization of neutral iron atoms leading to an underestimate by the LTE analysis of the Fe abundance from Fe I lines, Lind et al.'s (2012) extensive calculations of non-LTE effects across the Fe I spectrum did not unfortunately extend to an atmosphere representative of HD 179821. At  $T_{\text{eff}} > 7000$  K, models considered had  $\log g \geq 3$  and  $[Fe/H] \leq +0.25$ . A necessarily crude extrapolation suggests the LTE Fe abundance is underestimated by less than 0.1 dex. Species similar to Fe (e.g., Ni) will presumably be affected similarly and  $[X/Fe]$  will require an even smaller correction for non-LTE effects. We have not considered the role these effects play in determining the atmospheric parameters from Fe I and Fe II lines (Lind et al. 2012).

Non-LTE estimates for C, N, O, Na, Mg, Fe, Zn, and Ba appear to exhaust what has been published for warm supergiants such as HD 179821. In making this claim we have consulted the valuable review by Bergemann & Nordlander (2014) with its table of non-LTE studies of late-type stars. Many of the cited papers are concerned primarily or exclusively with the solar spectrum and several of the very recent papers focus on just five stars (Procyon, Arcturus,

HD 84937, HD 140283 and HD 122563) from which extrapolation to a supergiant like HD 179821 is most uncertain.

In the quest for more accurate abundance determinations for HD 179821, incorporation of non-LTE effects in the interpretation of the absorption lines and even in the construction of a model atmosphere may not provide the biggest leap to the end. The star's atmosphere violates the standard assumption of uniform plane-parallel (or spherical) layers in hydrostatic equilibrium. A supersonic macro-turbulence of  $22 \text{ km s}^{-1}$  starkly contradicts this assumption and challenges theoretical stellar astrophysicists to build more inclusive model atmospheres. The important STAGGER grid (Magic et al. 2013) does not intrude into the domain belonging to HD 179821; models at 7500 K refer to main sequence stars and the lowest gravity models ( $\log g = 1.5$ ) are no hotter than 4500 K. Realistic atmospheres of supergiants will have many applications including the extension of determination of analyses of supergiants to several galaxies beyond the Galaxy.

## 5 CONCLUDING REMARKS

There is no question but that HD 179821 is a luminous star. Possible identifications of the star include two possibilities: (i) a massive star evolving from the main sequence at approximately constant luminosity to the red supergiant phase or on a post-red supergiant loop back to the blue or (ii) a lower mass star evolving at roughly constant luminosity from the AGB to the tip of the white dwarf cooling track.

The mass-luminosity relations for these alternative identifications overlap for a range of masses. Above a certain luminosity, the more likely identification is a high mass star. This critical luminosity is set by the maximum mass – the Chandrasekhar mass – of a post-AGB star which may become a white dwarf. At the Chandrasekhar mass, the luminosity of a post-AGB star is  $M_{\text{bol}} \simeq -7.1$  or  $\log L/L_{\odot} \simeq 4.7$  (Wood, Bessell, & Fox 1983). Therefore, if it can be shown that HD 179821's luminosity exceeds the latter limit by a clear margin, one may identify the star as a massive star.

Estimations of HD 179821's absolute magnitude from an apparent magnitude are fraught with uncertainty owing to an uncertain correction for interstellar extinction with the possibility of an additional correction for circumstellar extinction. As previous investigators of the star have appreciated (Reddy & Hrivnak 1999; Kipper 2008; Oudmaijer et al. 2009), the absolute magnitude of HD 179821 may be estimated from the equivalent width (EW) of the O I triplet at 7770-7774 Å. The  $M_V - EW$  calibration for warm supergiants comes from Kovtyukh, Gorlova & Belik (2012) who assembled EW measurements for supergiants with known luminosities. Our measurement of the oxygen triplet's EW is 2.7 Å. Kovtyukh et al.'s calibration has few stars with such strong EW but mild extrapolation of the calibration gives  $M_V \simeq -8.9$  or  $\log L/L_{\odot} \simeq 5.5$ . This absolute magnitude is nearly two magnitudes brighter than the maximum for a post-AGB star and slightly fainter than the Humphreys-Davidson (Humphreys & Davidson 1979) limit of  $M_{\text{bol}} \simeq -9.5$  for the most luminous warm Galactic supergiants such as  $\rho$  Cas and HR 8752.

Absolute luminosities for post-AGB stars are poorly known, in general. Arellano Ferro, Giridhar, Arellano (2003)

<sup>8</sup>  $\Delta([Na/H]) = [Na/H]_{\text{NLTE}} - [Na/H]_{\text{LTE}}$

<sup>9</sup> The closest 1D model atmosphere is the ( $T_{\text{eff}}, \log g, [Fe/H]$ ) = (7250, 1.5, 0.5) model.

incorporated five post-AGB stars into their calibration of  $M_V - EW$  relation based primarily on normal supergiants. The two post-AGB star with estimated luminosities close to the luminosity limit for post-AGB stars had  $EW$ s of the triplet of 2.0 and 1.7 Å, values similar to  $EW$ s of normal supergiants of the same luminosity. Thus, it appears that normal supergiants and post-AGB stars of type F-G satisfy similar  $M_V - EW$  relations for the oxygen triplet.

The effective temperature and surface gravity provide a check on the conclusion that HD 179821 is a massive star. By combining the relations  $L \propto R^2 T_{\text{eff}}^4$  and  $g \propto M/R^2$ , one obtains

$$\log L/L_{\odot} = \log M/M_{\odot} + 4\log T_{\text{eff}} - \log g - 10.61 \quad (1)$$

On substituting  $T_{\text{eff}} = 7350\text{K}$ ,  $\log g = 0.64$  and  $\log L/L_{\odot} = 5.5$ , a mass  $M = 19M_{\odot}$  is obtained. Stellar evolutionary tracks (e.g., Iben 1985) imply that such a luminosity is achieved at a higher mass – say,  $30M_{\odot}$  – but an adjustment of  $\log g$  by just 0.2 dex provides just such a mass<sup>10</sup>.

It remains to consider HD 179821’s composition in light of the proposed identification as a massive star which has evolved beyond core H-burning on the main sequence to a He-core burning warm supergiant (and possibly beyond this phase!). A massive star observed as a warm supergiant may be expected to have shuffled at a minimum its C and N abundances as CN-processed material reached the surface by rotationally-induced mixing and the first dredge-up with the latter a contributor if the star is now evolving to the blue after a red supergiant phase. Present C/N/O abundances are taken from our analysis summarized in Table 6 with the approximate non-LTE corrections listed in Section 4.6, i.e., C = 8.5, N = 9.2 and O = 8.9. On the assumption that initial abundances satisfied the condition  $[X/\text{Fe}] = 0.0$  and  $[\text{Fe}/\text{H}] = +0.4$ , C = 8.9, N = 8.5 and O = 9.2 were the starting abundances; relative to these values N is clearly enriched, C and O are depleted. Assuming that the envelope has been mixed with CN-processed material from the interior, the CN-cycle’s catalysts of C and N are required to be conserved. The initial (logarithmic) sum is 9.0 and the observed sum is 9.3 with conservation satisfied within the measurement uncertainties and including the rough corrections for non-LTE effects. For more severe mixing, ON-cycled products may be involved and the conserved quantity is the sum of the C, N and O abundances. In this case, the initial value is 9.4 and the observed value is 9.3 which surely represents a case of fortuitous agreement. (Note: the analysis does not consider enhancement of the surface He abundance during evolution.)

Sodium overabundances in F-G supergiants have been the subject of several observational and theoretical investigations. As an observational reference point for HD 179821, we take the survey by Andrievsky et al. (2002) of Na abundances in F-G Ib-II giants which showed  $[\text{Na}/\text{Fe}]$  increasing with decreasing  $\log g$  reaching  $[\text{Na}/\text{Fe}] \simeq +0.3$  at

$\log g = 1.0$ . Non-LTE calculations show that the departures from LTE on the observed Na I lines at 6154 Å and 6160 Å are small ( $\sim 0.1$  dex) for supergiants with  $T_{\text{eff}} \sim 7000$  K. The Na enrichment is attributed to operation of the H-burning Ne-Na chain in which  $^{22}\text{Ne}$  is converted to  $^{23}\text{Na}$ . Denissenkov (2005) argued that observed levels of Na enrichment required massive stars to undergo mixing between core and the radiative envelope in their main sequence progenitor.

Inspection of Andrievsky et al.’s list of stars showed that just one was as Fe-rich as HD 179821. A reference sample of four stars was selected with the conditions that  $T_{\text{eff}} \geq 6500$  K and  $\log g \leq 1.0$ . For this quartet, mean values are  $[\text{Fe}/\text{H}] = -0.24$  and  $[\text{Na}/\text{Fe}] = +0.37$  with a small star-to-star scatter. If we assume that the  $^{22}\text{Ne}$  abundance scales with  $[\text{Fe}/\text{H}]$ , and the conversion of  $^{22}\text{Ne}$  to Na with subsequent mixing of Na to the surface are independent of metallicity, HD 179821 with  $[\text{Fe}/\text{H}] \simeq +0.4$  and  $[\text{Na}/\text{H}]$  also  $\simeq +0.4$  for an unmixed star is expected to have  $[\text{Na}/\text{Fe}] \sim 0.7$ , a value close to the observed value in Table 6.

An alternative identification of HD 179821 as a post-AGB star might appear to be excluded on the grounds that key signatures of post-AGB stars are absent, i.e., a C-rich and s-process atmosphere and envelope are clearly not a feature of HD 179821. This exclusion supposes that all AGB stars experience third dredge-up (i.e., envelope enrichment with C and s-process nuclides) before evolving off the AGB. The case of RV Tauri stars as post-AGB stars provides common examples of without carbon and s-process enrichment.

In such situations, when chemical composition is not a definitive way to distinguish massive evolved from post-AGB stars, other observed characteristics may be invoked. For example, the circumstellar CO expansion velocity for HD 179821 exceeds the typical velocity for post-AGB stars and likely requires a very luminous (i.e., a massive) star in order to drive the expansion by radiation pressure (Jura et al. 2001; Oudmajer et al. 2008). But, obviously, among the other characteristics the absolute luminosity plays a key role, one looks forward to a precise trigonometrical parallax. Until then, HD 179821 may be considered to be a warm Galactic supergiant like  $\rho$  Cas and HR 8752.

## ACKNOWLEDGMENTS

DLL thanks to the Robert A. Welch Foundation of Houston, Texas for support through grant F-634. VGK acknowledges the financial support by the Russian Foundation for Basic Research (project 14-02-00291a). TS thanks TUBITAK-BIDEP for financial support through its International Postdoctoral Research Scholarship Programme (1059B191500382). Christopher A. Sneden, Paul Barklem, Michel Breger, Earle Luck, Monika Adamow, Eswar B. Reddy, and Selçuk Bilir are acknowledged for helpful remarks on the manuscript and useful correspondence.

## REFERENCES

Andrievsky S. M., Egorova I. A., Korotin S. A., Burnage R., 2002, *A&A*, 389, 519

<sup>10</sup> An independent estimate of the mass was also provided by Parsec isochrones (Bressan et al. 2012) with the solar metal content of  $Z_{\odot} = 0.0152$  and using a  $Z = 0.03$  ( $[\text{Fe}/\text{H}] = \log(Z/Z_{\odot})$ ) isochrone (<http://stev.oapd.inaf.it/cgi-bin/cmd-2.7>). This isochrone, based on model atmosphere parameters reported in Section 4.2, provided a mass of  $30 M_{\odot}$  for HD 179821.

- Arellano Ferro A., Giridhar S., Rojo Arellano E., 2003, *RevMexAA*, 39, 3
- Arhipova V. P., Esipov V. F., Ikonnikova N. P., Komissarova G. V., Tatarnikov A. M., Yudin B. F., 2009, *Astron. Lett.*, 35, 764
- Arhipova V. P., Ikonnikova N. P., Noskova R. I., Sokol G. V., Shugarov S. Yu., 2001, *Astron. Lett.*, 27, 156
- Asplund M., Grevesse N., Sauval A. J., Scott P., 2009, *ARA&A*, 47, 481
- Barklem P. S., 2007, *A&A*, 466, 327
- Bensby T., Feltzing S., Oey M. S., 2014, *A&A*, 562, A71
- Bergemann M., Nordlander T., 2014, preprint (arXiv:1403.3088)
- Biémont E., & Godefroid M., 1980, *A&A*, 84, 361
- Boyarchuk A. A., Denisenkov P. A., Hubeny I., Ivanov V. V., Kubat I., Lyubimkov L. S., Sakhbullin N. A., 1988a, *IAU Colloq. 108: Atmospheric Diagnostics of Stellar Evolution*, 305, 94
- Boyarchuk A. A., Hubeny I., Kubat I., Lyubimkov L. S., Sakhbullin N. A., 1988b, *Astrophys.*, 28, 197
- Boyarchuk A. A., Hubeny I., Kubat I., Lyubimkov L. S., Sakhbullin N. A., 1988c, *Astrophys.*, 28, 202
- Boyarchuk A. A., Lyubimkov L. S., Sakhbullin N. A., 1985, *Astrophys.*, 22, 203
- Brand J., & Blitz L., 1993, *A&A*, 275, 67
- Bressan A., Marigo P., Girardi L., Salasnich B., Dal Cero C., Rubele S., Nanni A., 2012, *MNRAS*, 427, 127
- Castelli F., & Kurucz R. L., 2004, preprint (arXiv:astro-ph/0405087)
- Castro-Carrizo A., Quintana-Lacaci G., Bujarrabal V., Neri R., Alcolea J., 2007, *A&A*, 465, 45
- De Ruyter S., van Winckel H., Maas T., Lloyd Evans T., Waters L. B. F. M., Dejonghe H., 2006, *A&A*, 448, 641
- Den Hartog E. A., Lawler J. E., Sneden C., Cowan J. J., 2003, *ApJS*, 148, 543
- Denisenkov P. A., 2005, *ApJ*, 622, 1058
- Denisenkov P. A., & Ivanov V. V., 1987, *SvA Lett.*, 13, 214
- Fong D., Meixner M., Sutton E. C., Zalucha A., Welch W. J., 2006, *ApJ*, 652, 1626
- Führ J. R., & Wiese W. L., 2006, *J. Phys. Chem. Ref. Data*, 35, 1669
- Hannaford P., Lowe R. M., Grevesse N., Biémont E., 1982, *ApJ*, 261, 736
- Hinkle K., Wallace L., Valenti J., Harmer D., 2000, *Visible and Near Infrared Atlas of the Arcturus Spectrum 3727-9300 Å* ed. Kenneth Hinkle, Lloyd Wallace, Jeff Valenti, and Dianne Harmer. (San Francisco: ASP) ISBN: 1-58381-037-4, 2000.
- Hobbs L. M. et al., 2008, *ApJ*, 680, 1256-1270
- Howarth I. D., Phillips A. P., 1986, *MNRAS*, 222, 809
- Howarth I. D., Murray J., Mills D., Berry D. S., 1998, *Starlink User Note* 50
- Hrivnak B. J., Kwok S., Volk K. M. 1989, *ApJ*, 346, 265
- Humphreys R. M., & Davidson K., 1979, *ApJ*, 232, 409
- Iben I., Jr., 1985, *QJRAS*, 26, 1
- Jura M., & Werner M. W., 1999, *ApJ*, 525, 113
- Jura M., Velusamy T., Werner M. W., 2001, *ApJ*, 556, 408
- Kelleher D. E., & Podobedova L. I., 2008a, *J. Phys. Chem. Ref. Data*, 37, 1285
- Kipper T., 2008, *Baltic Astronomy*, 17, 87
- Klochkova V. G., Chentsov E. L., Tavolganskays N. S., Shapovalov M. V., 2007, *Astrophys. Bull.*, 62, 105
- Klochkova V. G., Panchuk V. E., Yushkin M. V., Nasonov D. S., 2008, *Astrophysical Bulletin*, 63, 386
- Korotin S. A., Andrievsky S. M., Hansen C. J., et al., 2015, *A&A*, 581, A70
- Kovtyukh V. V., Gorlova N. I., Belik S. I., 2012, *MNRAS*, 423, 3268
- Kurucz R. L., Furenlid I., Brault J., Testerman L., 1984, in Kurucz R. L., Furenlid I. Brault J. Testerman L., eds, *Solar Flux Atlas from 296 to 1300 nm*. National Solar Observatory, Sunspot, NM
- Lawler J. E., Bonvallet G., Sneden C., 2001a, *ApJ*, 556, 452
- Le Coroller H., Lebre A., Gillet D., Chapellier E., 2003, *A&A*, 400, 613
- Likkel L., Morris M., Omont A., Forveille T., 1987, *A&A*, 173, L11
- Lind K., Asplund M., Barklem P. S., Belyaev A. K., 2011, *A&A*, 528, A103
- Luck R. E. 2014, *AJ*, 147, 137
- Luck R. E., & Heiter U., 2007, *AJ*, 133, 2464
- Luck R. E., & Lambert D. L., 2011, *AJ*, 142, 136
- Ljung G., Nilsson H., Asplund M., Johansson S., 2006, *A&A*, 456, 1181
- Magic Z., Collet R., Asplund M., Trampedach R., Hayek W., Chiavassa A., Stein R. F., Nordlund A., 2013, *A&A*, 557, A26
- McWilliam A., 1998, *AJ*, 115, 1640
- Moultaka J., Ilovaisky S. A., Prugniel P., Soubiran C. 2004, *PASP*, 116, 693
- Munari U., Zwitter T., 1997, *A&A*, 318, 269
- Nave G., Johansson S., Learner R. C. M., Thorne A. P., Brault J. W. 1994, *ApJS*, 94, 2
- Nordhaus J., Minchev I., Sargent B., et al., 2008, *MNRAS*, 388, 716
- Osorio Y., & Barklem P. S., 2016, *A&A*, 586, A120
- Oudmaijer R. D., Davies B., de Wit W. J., Patel M., 2009, *The Biggest, Baddest, Coolest Stars*, 412, 17
- Panchuk V. E., Klochkova V. G., Yushkin M. V., Najdenov I. D., 2007, in Gomez de Castro A. I., Barstow M. A., eds, *Proceedings of the Joint Discussion No. 4 during the IAU General Assembly of 2006, The UV Universe: stars from birth to death*. Editorial Complutense, Madrid, p.179
- Panchuk V. E., Klochkova V. G., Yushkin M. V., and Naidenov I. D., 2009, *J. Opt. Technol.*, 76, 42
- Podobedova L. I., Kelleher D. E., Wiese W. L., 2009, *J. Phys. Chem. Ref. Data* 38, 171
- Reddy B. E., Hrivnak B. J., 1999, *AJ*, 117, 1834
- Schwarzschild M., 1975, *ApJ*, 195, 137
- Scott P., Asplund M., Grevesse N., Bergemann M., Sauval A. J., 2015, *A&A*, 5
- Sneden C., 1973, PhD thesis, Univ. of Texas at Austin, USA
- Sobeck J. S., Lawler J. E., Sneden C., 2007, *ApJ*, 667, 1267
- Stobie R. S., 1977, *MNRAS*, 180, 631
- Şahin T., 2008, Ph.D. Thesis, Queen's University Belfast
- Şahin T., Lambert D. L., Klochkova V. G., Tavolganskaya N. S., 2011, *MNRAS*, 410, 612
- Takeda Y., & Takada-Hidai M., 1998, *PASJ*, 50, 629
- Takeda Y., Hashimoto O., Taguchi H., Yoshioka K., Takada-Hidai M., Saito Y., Honda S., 2005, *PASJ*, 57, 751
- Thévenin F., 1989, *A&AS*, 77, 137



- Thévenin F., & Idiart T. P., 1999, *ApJ*, 521, 753  
Thévenin F., Parthasarathy M., Jasiewicz G., 2000, *A&A*, 359, 138  
Tull R. G., 1998, *SPIE*, 3355, 387  
Tull R. G., MacQueen P. J., Sneden C., Lambert D. L., 1995, *PASP*, 107, 251  
van der Veen, W. E. C. J., Habing H. J., Geballe, T. R. 1989, *A&A*, 226, 108  
van der Veen W. E. C. J., Trams N. R., Waters L., 1993, *A&A*, 269, 231  
Venn K. A. 1995, *ApJ*, 449, 839  
Wiese W. L., Fuhr J. R., Deters T. M., 1996, *J. Phy. Chem. Ref. Data*, Monograph No. 7  
Wood P. R., Bessell M. S., Fox M. W., 1983, *ApJ*, 272, 99  
Wood M. P., Lawler J. E., Sneden C., Cowan J. J., 2013, *ApJ*, 208, 27  
Yushkin M. V., Klochkova V. G., 2005, Preprint *Spec. Astrophys. Obs.*, No. 206, pp. 1-61 SAO  
Začs L., Klochkova V. G., Panchuk V. E., Spelmanis R., 1996, *MNRAS*, 282, 1171  
Zuckerman B., Dyck H. M., 1986, *ApJ*, 311, 345

**APPENDIX A: EQUIVALENT WIDTH  
MEASUREMENTS OF NEUTRAL AND  
IONIZED FE LINES OVER THE 18 EPOCHS  
LISTED IN TABLE 1.**

**Table A1.** Equivalent width measurements of neutral and ionized Fe lines over the 18 epochs listed in Table 1.

Wave. (Å)	Spec.	LEP (eV)	loggf	EW	EW	EW	EW	EW	EW	EW	EW	EW
				15Oct97 (mÅ)	13Sep00 (mÅ)	21Apr08 (mÅ)	13Jun08 (mÅ)	11Jul08 (mÅ)	10Aug08 (mÅ)	17Aug08 (mÅ)	17Sep08 (mÅ)	14Apr09 (mÅ)
4484.23	26.0	3.60	-0.86	...	89.7	89.4	118.6	120	128.8	...	...	...
4602.95	26.0	1.49	-2.22	277.70	142.9	152.3	156.3	152.7	136.5	119.6	...	...
4643.47	26.0	3.65	-1.15	46.30	28.5	37.8	47.1	32.5	51.1	29.9	...	...
5090.77	26.0	4.26	-0.44	76.70	73.8	54.3	105.1	98.9	118.4	87.9	...	...
5353.37	26.0	4.10	-0.68	103.90	55.6	64.0	77.9	...	70.4	66.2	45.6	63.6
5364.88	26.0	4.45	0.23	209.00	148.8	145.0	167.4	158.0	152.4	147.4	117.3	134.2
5367.48	26.0	4.42	0.44	215.40	144.6	196.0	172.5	161.0	154.7	149.8	137.3	160.5
5373.71	26.0	4.47	-0.84	...	14.8	12.4	17.4	21.6	19.3	21.9	11.4	24.0
5393.18	26.0	3.24	-0.72	...	103.7	147.7	130.9	128.9	121.8	114.5	88.4	180.9
5434.53	26.0	1.01	-2.12	273.50	213.4	284.9	257.9	213.0	228.3	213.5	190.3	226.2
5569.63	26.0	3.42	-0.49	175.20	108.9	135.0	152.9	143.2	138.5	137.5	107.5	119.8
5572.85	26.0	3.40	-0.28	178.00	154.4	194.8	201.9	187.7	178.7	181.7	162.1	179.6
5816.38	26.0	4.55	-0.60	33.30	36.0	38.0	33.6	30.4	26.3	35.7	21.2	26.8
6020.17	26.0	4.61	-0.21	57.30	28.9	42.5	48.7	54.6	41.1	...	27.8	39.0
6024.07	26.0	4.55	-0.06	101.10	68.3	87.3	94.8	92.2	82.2	...	68.2	77.6
6027.06	26.0	4.08	-1.09	51.70	25.6	42.9	46.3	43.6	34.8	...	22.8	32.2
6065.49	26.0	2.61	-1.53	...	52.9	64.6	80.2	63.6	60.2	...	34.0	50.5
6393.61	26.0	2.43	-1.58	...	...	91.0	99.1	82.6	76.3	...	47.0	60.4
6411.66	26.0	3.65	-0.72	...	70.1	88.1	101.1	91.8	86.1	...	68.9	76.9
6592.91	26.0	2.73	-1.47	...	...	70.5	97.2	57.2	60.9	...	...	47.8
6841.34	26.0	4.61	-0.60	...	...	37.8	42.6	39.5	36.8	...	...	...
4893.82	26.1	2.83	-4.27	272.30	222.9	228.5	229.8	212.7	211.9	221.8	...	...
5427.80	26.1	6.72	-1.58	74.10	94.6	115.5	86.9	74.0	72.0	89.1	83.0	76.6
5813.67	26.1	5.57	-2.75	68.40	65.6	83.2	83.9	78.4	79.2	85.5	85.0	77.6
5823.18	26.1	5.57	-2.99	59.10	33.0	47.1	66.8	48.7	45.7	49.9	37.9	54.3
5991.38	26.1	3.15	-3.65	242.60	...	215.8	295	245.2	250.6	239.1	248.1	253.5
6113.33	26.1	3.22	-4.23	133.70	125.8	135.1	145.7	130.5	131.6	...	129.4	138.9
6129.73	26.1	3.20	-4.74	118.80	103.1	90.1	104.1	96.4	87.7	...	72.4	67.3
6179.40	26.1	5.57	-2.80	...	85.4	76.8	82.4	58.0	69.1	...	56.8	66.6
6446.40	26.1	6.22	-2.08	...	...	86.0	97.5	98.7	104.6	...	74.9	92.9

**Table A2.** Equivalent width measurements of neutral and ionized Fe lines over the 18 epochs listed in Table 1.

Wave. (Å)	Spec.	LEP (eV)	loggf	EW	EW	EW	EW	EW	EW	EW	EW	EW	EW
				9May09 (mÅ)	7Nov09 (mÅ)	21Nov09 (mÅ)	22May10 (mÅ)	3Jun10 (mÅ)	30Jul10 (mÅ)	24Sep10 (mÅ)	17Nov10 (mÅ)	16May11 (mÅ)	27Aug13 (mÅ)
4484.23	26.0	3.60	-0.86	102.8	...	174.2	167.1	...	74.8	...	...	151.2	182.9
4602.95	26.0	1.49	-2.22	151.2	...	146.6	197.6	...	115.1	...	...	155.6	188.6
4643.47	26.0	3.65	-1.15	47.8	...	34.3	45.8	...	20.4	...	...	36.3	55.0
5090.77	26.0	4.26	-0.44	101.1	...	115.0	121.2	...	60.9	...	...	69.5	110.3
5353.37	26.0	4.10	-0.68	77.2	60.7	69.0	102.6	93.3	56.0	70.4	94.7	72.4	97.7
5364.88	26.0	4.45	0.23	157.0	147.5	179.8	192.0	181.5	121.1	148.0	218.8	178.7	203.0
5367.48	26.0	4.42	0.44	190.7	146.4	160.3	188.1	188.0	140.6	158.9	221.0	168.1	194.0
5373.71	26.0	4.47	-0.84	26.5	15.9	27.4	...	26.6	24.7	19.7	22.5	27.1	36.7
5393.18	26.0	3.24	-0.72	133.9	98.9	126.6	168.7	153.1	102.5	112.0	157.0	127.2	159.4
5434.53	26.0	1.01	-2.12	234.4	218.0	196.6	316.9	315.2	200.1	238.8	301.7	230.0	285.6
5569.63	26.0	3.42	-0.49	149.4	126.5	143.4	154.0	175.7	...	137.5	176.6	148.5	187.9
5572.85	26.0	3.40	-0.28	209.4	194.2	185.6	227.1	219.5	...	181.9	224.0	199.6	230.5
5816.38	26.0	4.55	-0.60	35.0	...	23.8	45.0	34.8	...	27.1	39.1	28.4	37.9
6020.17	26.0	4.61	-0.21	56.9	...	46.5	66.4	62.1	...	43.7	75.1	46.2	87.9
6024.07	26.0	4.55	-0.06	96.8	...	96.4	107.6	102.8	...	87.5	108.3	85.1	118.6
6027.06	26.0	4.08	-1.09	43.5	...	33.3	59.5	52.0	...	33.3	52.8	39.1	55.8
6065.49	26.0	2.61	-1.53	70.0	...	65.1	93.4	93.5	...	62.1	87.9	60.9	91.9
6393.61	26.0	2.43	-1.58	87.3	...	83.3	124.7	112.4	...	70.9	119.2	68.8	94.6
6411.66	26.0	3.65	-0.72	98.6	66.6	88.9	111.8	100.3	...	86.6	104.8	87.4	130.3
6592.91	26.0	2.73	-1.47	71.7	...	58.7	106.9	87.7	...	64.6	102.0	68.1	...
6841.34	26.0	4.61	-0.60	50.3	...	18.8	40.1	...	...	...	...	51.3	...
4893.82	26.1	2.83	-4.27	238.5	...	228.4	212.5	...	230.1	...	...	252.2	266.1
5427.80	26.1	6.72	-1.58	91.1	80.9	95.4	91.0	85.4	98.1	81.1	95.7	88.3	101.7
5813.67	26.1	5.57	-2.75	86.4	...	83.7	93.1	70.9	...	88.3	82.8	94.9	87.1
5823.18	26.1	5.57	-2.99	67.9	...	44.4	63.2	50.8	...	38.5	46.0	42.3	49.2
5991.38	26.1	3.15	-3.65	223.0	...	266.0	281.5	286.0	...	240.7	264.4	268.7	...
6113.33	26.1	3.22	-4.23	137.7	...	145.4	147.2	152.2	...	133.5	143.4	132.6	...
6129.73	26.1	3.20	-4.74	111.0	...	105.6	118.2	...	...	89.8	101.8	95.5	106.5
6179.40	26.1	5.57	-2.80	69.4	...	76.3	68.3	74.7	...	71.2	80.6	80.2	92.7
6446.40	26.1	6.22	-2.08	89.4	89.6	97.1	103.2	91.5	...	85.4	86.6	74.3	...